Power Spectrum Density Estimation Methods for Michelson Interferometer Wavemeters

By

Apoorva Mulye

Thesis submitted to the
Faculty of Graduate and Postdoctoral Studies
in partial fulfillment of the requirements for the degree of
Master of Applied Science
in Electrical and Computer Engineering

Ottawa-Carleton Institute for Electrical and Computer Engineering
School of Electrical Engineering and Computer Science
Faculty of Engineering
University of Ottawa
2016

Abstract

In Michelson interferometry, many algorithms are used to detect the number of active laser sources at any given time. Conventional FFT-based non-parametric methods are widely used for this purpose. However, non-parametric methods are not the only possible option to distinguish the peaks in a spectrum, as these methods are not the most suitable methods for short data records and for closely spaced wavelengths. This thesis aims to provide solutions to these problems. It puts forward the use of parametric methods such as autoregressive methods and harmonic methods, and proposes two new algorithms to detect the closely spaced peaks for different scenarios of optical signals in wavemeters. Various parametric algorithms are studied, and their performances are compared with non-parametric algorithms for different criteria, e.g. absolute levels, frequency resolution, and accuracy of peak positions. Simulations are performed on synthetic signals produced from specifications provided by our sponsor, i.e., a wavemeter manufacturing company.

Acknowledgements

This thesis has been a wonderful journey. People from various quarters have helped me to traverse the path towards my thesis.

My deepest gratitude go to my Research Supervisor Professor Martin Bouchard for his constant support, guidance and critiques on my work. He has always been very generous with his time and efforts. I learnt many basic things in depth in a Digital Signal Processing course offered by him. I cannot thank him enough for guiding me throughout my thesis, being patient with me and supporting me when I was going through difficult times. Working under your supervision has been the most wonderful experience of my life and it will have a great impact on my future endeavours as well. Thank you for giving me a chance to be a part of your research team.

I would like to thank Professor Eric Dubois who gave two interesting graduate courses Adaptive Signal Processing and Image processing which helped me gain more knowledge in my research field.

I would like to thank our sponsor company Simbol Test Systems Inc. for the financial support that I received during my studies. Thanks to Professor Shervin Shirmohammadi for recruiting me as a Teaching Assistant for his graduate level course Computer Communication Networks.

A special thanks to my roommates Vipul, Shwetank, Deepansh and Chirag Bhai who supported and motivated me to achieve my goal when I was down.

I am very grateful to my sister Vaishali and my brother in law Nitant. They helped me to settle down in a new country and have been looking after me from the very first day. I am truly and deeply indebted to them, the numerous motivating and inspiring discussions I had with them and for giving me their affection. This journey wouldn't have been the same without your love and support. Thank you for being my family away from home!

Finally, I would like to thank my parents and my brother Amod for their continued support and who were the most thrilled at my decision to pursue Masters studies. I would like to thank my father Mr. Dinkar Mulye for supporting me financially through the course and has never asked anything in return. I would like to thank my mother Mrs. Anagha Mulye for her blessings and for being a main source of encouragement and emotional support.

Without my family's love and support, I would be nowhere!

Table of Contents

List of Figures

List of Tables

List of Acronyms

AR	Autoregressive
ARMA	Autoregressive Moving Average
DFT	Discrete Fourier Transform
ESPRIT	Estimation of Signal Parameters via Rotational Invariance Techniques
FFT	Fast Fourier Transform
FTIR	Fourier Transform Infrared Spectrometry
FTS	Fourier Transform Spectrometry
FWHM	Full Width at Half Maximum
MA	Moving Average
MUSIC	MUltiple SIgnal Classification
PSD	Power Spectrum Density
SNR	Signal to Noise Ratio
WSS	Wide Sense Stationary

Chapter 1 Introduction

1.1 Motivation and previous work

Wave characteristics such as interference of electromagnetic (EM) waves find many applications in medicine, science and technology. Random noise addition to the signal makes many techniques inappropriate for application of accurate measurement. Interferometers are useful for signal requiring a non-invasive and applications that don't require any contact. This allows to avoid physical contact with a measured object which may lead to spurious signals. Fourier transform spectrometers are widely used today for various purposes such as food analysis, petrochemicals, pharmaceuticals, polymer industry, optical fibres etc. Fourier transform spectrometry (FTS) makes use of Fourier transforms to measure the spectrum [KAU'01], [MIC]. The Fourier transform converts interferograms into actual spectrum. Interferometers were first invented to study light speed and to fix the standard meter with the wavelength of a spectral line. This interferometer was first invented by A.A.Michelson. Later on this type of interferometer was used as a spectrometer. FTS has numerous advantages over dispersive spectrometers which are discussed later. A major advantage is that Michelson interferometers monitor all wavelengths simultaneously for the whole measurement procedures, which in turn allows an increased signal to noise ratio (SNR). It does not require a limited aperture which is beneficial for incident light which is not of a single spatial mode [KAU'01], [MIC], [YUE'07].

The Michelson interferometer used for this thesis is for the purpose of a multiline optical channel analyzer. This instrument has the ability to measure and differentiate the absolute wavelengths of up to 256 optical signals [MUL]. This interferometer usually works on the conventional Fourier transform or Fast Fourier transform (FFT) method in order to provide the full optical display. However, FFT or Fourier transform methods are not necessarily the best possible option to display the spectrum. Linear combinations of sinusoidal and complex exponential signals lead to the Fourier transform and the frequency domain characterization of signals. These techniques provide useful representations of signals because of their generality. However, these techniques are not the most efficient representation of signals with a known structure. Along with this, spectra provided by this method tend to hide weak peaks or don't display closely spaced wavelength peaks due to the spectral leakage of windows used in this process. These methods don't work well with short data records and are limited in their ability to resolve close wavelengths in such cases [HAY'97], [PRO'96], [STO'05].

Therefore, in the context Michelson interferometry there is a necessity to work on other power spectrum density estimation (PSD) methods which provide a better display with a good resolution even for shorter

data records. Several studies have been done to overcome the problems suffered in Fourier transform based power spectrum estimations [UBE'03], [SUB'06]. These methods are divided mainly into two methods: 1) Non-parametric methods 2) Parametric methods.

PSD estimation is an area which has a lot of applications in real time real life signals and extensive research has been done on this area of the signal processing. Most of the work deals with new algorithms and techniques as well as modifications of existing techniques. The rest of the work is related to the understanding of abilities and limitations of PSD techniques. The analysis of performance of non-parametric methods is easy to compute and understand, whereas performance analysis of parametric methods is more difficult to conduct. This is one of the reasons that non-parametric methods are widely used compared to parametric methods, even though considerable amount of research has been done on parametric methods [PRO'96], [PER'06], [MAN'05].

Most commonly used methods are based on the periodogram which is a non-parametric method introduced by Schuster (1898) while studying for periodicities in sunspot numbers. But as further research were done, it was shown that although the periodogram is easy to compute, for short data records its ability to produce an accurate estimate of PSD is limited. One of the shortcomings of the periodogram method is that its mean value has a bias which means the estimated PSD has a distortion and thus does not represent true PSD. This in turn lead to smoothing effects and spectral leakage due to the windows used. This limits the ability to distinguish closely spaced wavelengths. Moreovever, the variance of the periodogram estimate does not decay even if a large number of samples is used, thus the periodogram is not a consistent estimate of PSD. These limitations were somehow rectified in some non-parametric methods [PRO'96], [PER'06], [MAN'05], [CAS'11], [AYE'03].

Non-parametric methods estimate an autocorrelation sequence from a given set of data and then by taking the Fourier transform of this sequence to obtain a consistent estimate of PSD through averaging or smoothing of the autocorrelation sequence or the periodogram. Non-parametric methods include the Bartlett method, the Welch method and the Blackman Tukey method [PRO'96], [BEL'01].

The Bartlett method divides an N-point sequence into K non-overlapping sequence each of fixed length, and a periodogram of each is computed. An average of all the K segments periodogram is taken to estimate the final PSD. The Welch method is similar to the Bartlett with some modifications that the overlapping of subdivided sequence is allowed and window is applied to each segment before taking the actual periodogram of each segment, which are then combined to get the estimated PSD. The Blackman Tukey method windows the autocorrelation of the samples and a Fourier transform of these is taken to get the PSD estimate [HAY'97]. All these methods are discussed in detail later in this thesis.

One of the main limitation of non-parametric methods is that they don't incorporate into the estimation technique information that may be available about the process. In many applications such as the case considered in this thesis, this may be an important limitation where knowledge is available about how the data samples are generated. By using parametric methods for PSD estimation, better and more accurate resolution of PSD estimates can sometimes be found. There are main four processes used in parametric methods which are: 1) Autoregressive (AR) 2) Moving Average (MA) 3) Autoregressive moving average (ARMA) 4) Harmonic (complex exponential in noise) [OPP'09], [HAY'97]. Autoregressive and harmonic models suit best the kind of signals used for this thesis' purpose, i.e., very narrowband optical sinusoidal carriers.

AR processes represent narrow peaks efficiently and are easy to implement. The main methods used in AR processes are 1)Yule-Walker 2)Burg 3) Minimum covariance 4) Covariance. Harmonic methods are used for the case of complex sinusoids in noise. Later in the thesis, it is shown that the harmonic methods give the best output in terms of frequency resolution [PER'06], [SUB'06], [UBE'03], for the signals considered in this thesis. The different types of harmonic methods are as follows:1) MUSIC method 2) ESPRIT Method 3) Pisarenko Harmonic Decomposition Method. These methods along with AR methods are also explained in details later in the thesis.

Some experiments were done with the existing methods and a few modifications were also done to the existing methods in order to achieve the best PSD in terms of frequency resolution, to detect closely spaced peaks. A couple of new algorithms were proposed and tested in the thesis and were found to be working properly for the desired application.

As Michelson interferometers deal with optical signals, its is common to work on the wavelengths instead of the frequencies while doing the experiments. Another difference with standard PSD estimation in this project is that sampling and generation of the signals is in the space domain rather that the time domain. Thus it also required to learn a few basic things regarding the interferometer instrument. Samples obtained in this kind of interferometer are generated according to the movement of a movable mirror, i.e., the optical path change.

The company Simbol Test Systems Inc. were the sponsor for this thesis. All the work was timely given to the company for real life application, and developments in the PSD algorithms were done according to their specifications, typically to match or outperform the commercial Exfo WA-7600/7100 wavemeter [MUL].

1.2 Thesis objectives and organization

The main goal and the theme of the research is to come up with the best working PSD methods that help to achieve better frequency resolution display for detection of closely spaced peaks. The objective of this thesis is to improve the performance of a wavemeter, whose main purpose is to determine the number of active laser channels/sources at any particular moment. In order to do so using a signal provided by a Michelson interferometer, an appropriate frequency resolution between the sources/channels is necessary to distinguish the frequencies. Based on this research theme, the following are the major objectives of the thesis:

- to provide a basic review of the working of Michelson interferometers, non-parametric PSD estimation methods, and parametric/harmonic PSD estimation methods;
- to analyze the literature and identify methods for improving the performance of the wavemeter to detect the active number of laser sources;
- to compare the results/performance of different methods (frequency resolution, accuracy of frequency/wavelength, absolute level wherever needed) for the optical signals found in our application of interest;
- to further investigate and compare performance of the selected methods for different scenarios i.e. peak locations, determining the number of peaks in a particular waveband and using different windows;
- to further develop and evaluate new methods for better frequency content display and compare with existing algorithms.

To achieve these objectives, the thesis is organized in the following way:

Chapter 2 provides some review of the Michelson interferometer. It explains the working of this interferometer, its construction and the physics behind its working.

Chapter 3 describes the basics of various non-parametric methods and their mathematics along with the zoom FFT method which were tested for this thesis and studied during the literature survey.

Chapter 4 gives the details of parametric power spectrum estimation techniques. Harmonic methods which are used for this thesis are also explained in this chapter. It also gives some overview of the new proposed algorithms.

Chapter 5 evaluates all the considered parametric, non-parametric, harmonic methods and a couple of new proposed methods. Simulations done for parametric methods are explained first. Results of these simulation are explained and compared with the simulation results of non-parametric methods. All the parametric methods and harmonic/MUSIC methods are compared to each other using these results. Further evaluation is done of all the best possible methods based on results obtained in different scenarios in terms of frequency resolution, positions of wavelength peaks and in some cases absolute level. The new proposed "MIX FFTs" and "MIX FFT and MUSIC" methods are also explained.

Chapter 6 provides some discussions based on the experiments and the results. A few conclusions are made based on the work done and the results of these methods to explain the suitability of these methods, and few observations are explained.

Chapter 7 gives summary of the thesis and provides some direction for future research work based on the thesis.

1.3 List of contributions

The following are the major contributions of the thesis:

- the basics of the Michelson interferometer, of non-parametric PSD estimation methods and parametric PSD estimation methods are reviewed and explained in Chapter 2, 3 and 4 respectively;
- Simulations are done to compare in Chapter 5 the performance of different parametric, harmonic and non-parametric PSD estimation methods, for PSD estimation from short sequences provided by Michelson interferometers with optical signals;
- the introduction and evaluation in Chapter 5 of two new proposed algorithms which are the "MIX FFTs" and the "MIX FFT and MUSIC" methods, as well as a comparisons of these methods with conventional parametric methods;
- the production of real-time C-code and DLL libraries. This work was done as part of a research contract with a company. In addition to Matlab simulations and results provided in this thesis, C code and DLL libraries were also produced in order for the algorithms to be incorporated in the real-time code of a practical wavemeter. The main libraries used for the development of the C code are PFFT which is an extension of FFTPACK, and CLAPACK for matrix operations (mostly for eigenvalue decompositions). C code and DLL libraries developed for this thesis are currently being

used by the sponsor company in a practial Michelson Interferometer wavemeter instrument. For code validation, it was verified that all the plots generated using MATLAB codes were also obtained when the C code was used.

Chapter 2 Overview of Michelson Interferometer

2.1 Basics of Michelson Interferometer

Infrared spectrometers form the basis of Fourier transform infrared spectrometers (FTIR). The infrared range can be divided into near infrared region (12800~4000cm^{-1}), mid infrared region (4000~200cm^{-1}) and far infrared region (50~1000cm^{-1}). These spectrometers are the third generation infrared spectrometers [UCD]:

1) In the late 1950s the first generation of IR spectrometer was invented which used prism optical splitting systems. These prisms are composed of NaCl. Some of the disadvantages of these early spectrometers is that their scan range is very narrow. Also, repeatability was very poor.

2) A second generation IR spectrometer was invented in 1960s. Grating is used as a monochrometer. The second generation spectrometer provides better performance than the first generation spectrometer. But it also suffers from a few disadvantages. It has a low scan speed, poor wavelength accuracy and low sensitivity.

3) The third generation is the Fourier transform infrared spectrometer which doesn't use a monochrometer, thus enhancing its performance over the previous generations. The main advantages of FTIR spectrometers are:

1) Wavenumber accuracy is high with an error in the range of ±0.01 cm^{-1} ;

2) Its signal to noise ratio (SNR) is higher than the previous IR spectrometers;

3) It provides extremely high resolution (0.1~0.005 cm^{-1});

4) It has a reduced interference from stray light;

5) It has a wide scan range (1000~10 cm^{-1});

6) The scan time of all frequencies is short, with typically around 1s.

Fourier transform spectrometry (FTS) forms the spectrum using Fourier transform techniques. The Michelson interferometer is the most widely used FTS instrument. This type of interferometer was

developed by Michelson in 1880s. It consists of two optical beams (with the help of beamsplitter) and two plane mirrors [KAU'01], [YUE'07]. Although, this instrument was invented a long way back, it was first used for computing the spectrum in 1949 by astrophysicist Peter Fellgett. Michelson interferometer find many applications in optical coherence tomography (OCT), astronomical interferometry, detection of gravitational waves, studies of atmosphere etc. A common application of this instrument is in dense wavelength division multiplexing (DWDM) to measure accurately the optical wavelength to characterize and optimize DWDM components and transmission systems. It is used to detect wavelengths of numerous optical carriers multiplexed on a single optical fiber such as optical fibers used in telecommunication. The Michelson interferometer used in this thesis serves this purpose i.e. to detect the active number of laser sources in an optical fiber used in the telecommunication industry [MUL]. The instrument is made up of a measurement and reference channel consisting of He-Ne laser which has 10^{-8} relative frequency stability and 10^{-7} relative frequency reproducibility. The measurement laser wavelength is calculated by counting the interference fringes from the measurement and reference lasers. By collecting the analog signal of measurement light with a sampling time scale based on the interference fringes pulses, the optical spectrum of measurement light can be obtained [YUE'07], [UCD]. Before discussing the working and construction of a Michelson interferometer, it is necessary to introduce some physics regarding light interference [YUE'07], [KAU'01].

A monochromatic electromagnetic wave is modeled as,

$$E = Ae^{i(\mathrm{k}.\mathrm{r}-\omega \mathrm{t})} \tag{2.1}$$

where,

E is an electric field strength, A is amplitude, r is position vector, k is a wavenumber, t is time and ω is an angular frequency. Now, the wavenumber k can be given as,

$$k = \frac{2\pi}{\lambda} = 2\pi\nu \,, \tag{2.2}$$

where,

λ is the EM wave's wavelength and ν is a wavenumber expressed in 1/cm or 1/m. The optical path difference/distance between interference fringes in the interferometer in air or vacuum is a function of a wavenumber. Even though wavelength is the standard used in the industry, wavenumbers which are analogous to frequency are used for spectral analysis. As the angular frequency is extremely high, E

cannot be measured as a function of time. Instead, the intensity, i.e., power, of the EM wave per area is measured.

$$I \propto A^2 \tag{2.3}$$

Two EM waves propagating in the same direction 'x' with a phase difference of δ can be modeled as,

$E_1 = A_1 e^{i(\mathrm{k}_x x - \omega \mathrm{t})}$ and $E_2 = A_2 e^{i(\mathrm{k}_x x - \omega \mathrm{t} + \delta)}$. The interference of the waves is shown in figure (2.1).

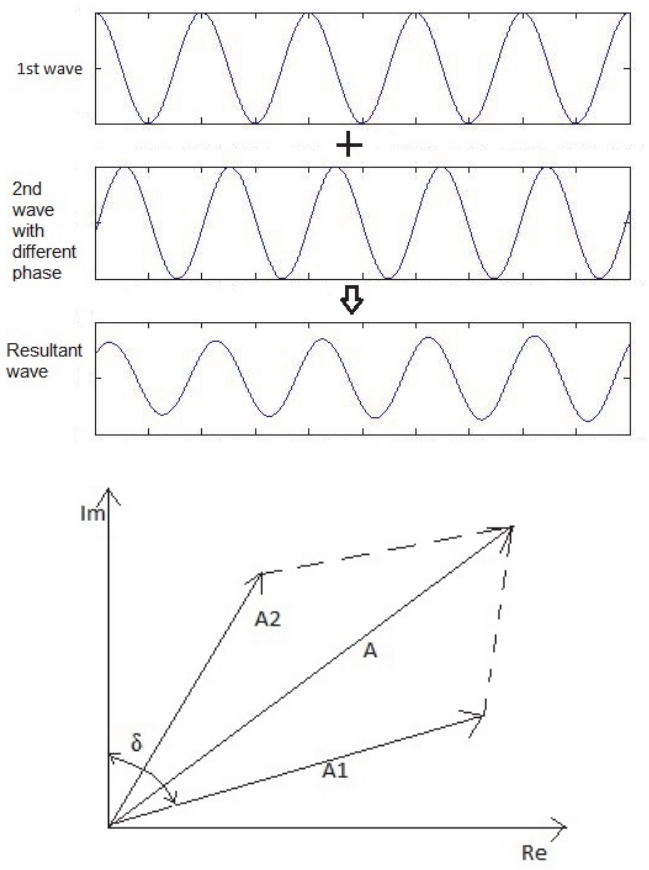

Figure 2.1:Interference of two waves, A is the resultant amplitude

This interference of the waves produces a wave whose amplitude square is as follows,

$$A^2 = A_1^2 + A_2^2 + 2A_1 A_2 \cos\delta \tag{2.4}$$

The intensity of this wave is,

$$I = I_1 + I_2 + 2\sqrt{I_1 I_2}\cos\delta \tag{2.5}$$

and for $I_0 = I_1 = I_2$

$$I = 2I_0(1+\cos\delta) \tag{2.6}$$

Equation (2.6) holds true when both the wave that are interfering have equal intensity, $I_0 = I_1 = I_2$.

2.2 Construction and working of an interferometer

The Michelson interferometer is very simple FTS. One beam of light is divided into two beams with different paths. These two beams are then combined by the Michelson interferometer and the intensity difference of these two beams is calculated as a function of different paths at the detector. This can be seen from the figure below :

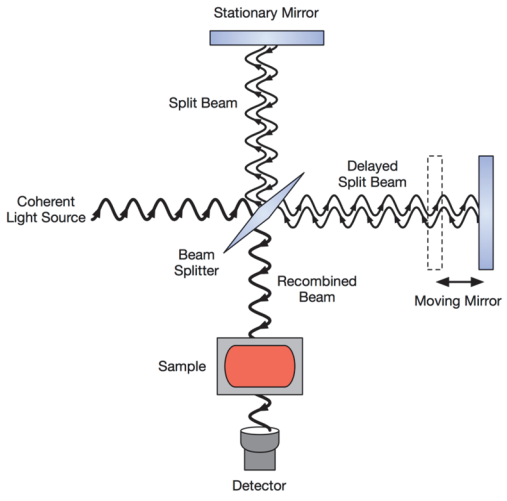

Figure 2.2:Michelson Interferometer schematic diagram

The Michelson interferometer consists of a beamsplitter and two perpendicular mirrors, one of which is a movable and the other one is a stationary mirror. The beamsplitter reflects half of the light and transmits

half of the light. The reflected light and transmitted light hit the movable and stationary mirror respectively and the reflected lights from the mirrors are interfered at the beamsplitter [KAU'01], [UCD], [MIC].

The Michelson interferometer produces two images P' and P" of a real source S_0. This is illustrated in figure (2.3). $S_0^{'}$ and $M_2^{'}$ are the image of the source and the moving mirror, respectively. Mirror M_1 forms the image of $S_0^{'}$ which is P', and mirror $M_2^{'}$ forms the image of $S_0^{'}$ which is P". Let the distance between mirror M_1 and mirror $M_2^{'}$ be d, the distance between images P" and P' is then $2d$.

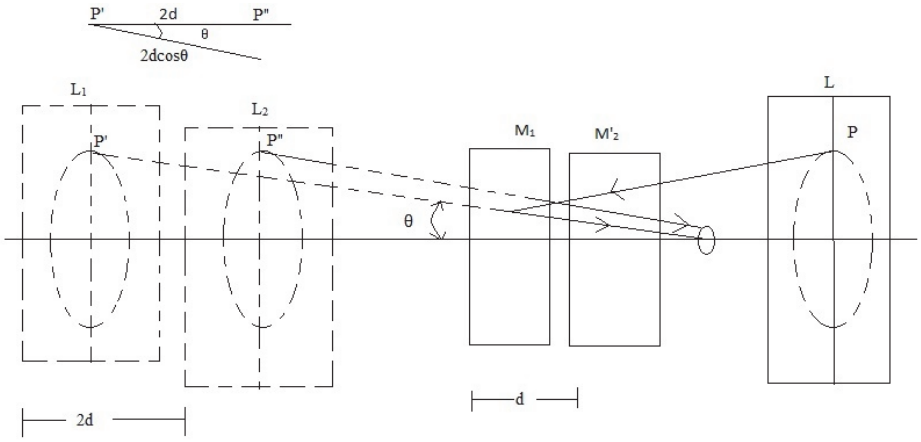

Figure 2.3:Interference pattern formed by a Michelson Interferometer

2.3 Physics of Interferometer

From Figure 2.3 it can be seen that rays travel with respect to an optical axis at an angle θ. The optical path difference of the rays coming from two coherent images is,

$$x = 2nd\cos\theta \tag{2.7}$$

where, n is the refractive index of the medium. The phase difference of the two rays can be given as,

$$\delta = \frac{2\pi x}{\lambda} = \frac{2\pi}{\lambda} 2nd\cos\theta \tag{2.8}$$

The intensity maxima of an interference pattern is obtained with the conditions:

$\delta = l2\pi$, $\quad l = 0, \pm 1, \pm 2, \ldots$

$$2nd\cos\theta = l\lambda \qquad l = 0, \pm 1, \pm 2, \ldots \tag{2.9}$$

Now, if rays propagate in the direction of the optical axis i.e. θ=0 , S_0 is a monochromatic light source and the medium is vacuum i.e. n =1, then the optical path difference of two rays is $x = 2d$ and its intensity is given by:

$$F = 2I_0[1 + \cos(2\pi x/\lambda)] \tag{2.10}.$$

This intensity is a function of the distance d and the maxima are obtained in intervals $\lambda/2$ of the distance d.

Considering that the light source S_0 is continuous with a wide range of wavenumbers, such that the beam in both branches of the interferometer is E(ν) which is a spectrum. The interference signal from the infinitesimal spectral band of $\nu + d\nu$ for an optical path difference x is:

$$dF(x,\nu) = 2\,E(\nu)[1+\cos(2\pi\nu x)]\,d\nu \tag{2.11}.$$

The total signal of the whole spectral band is:

$$F(x) = 2\int_0^\infty E(\nu)[1 + \cos(2\pi\nu x)]d\nu \tag{2.12}.$$

This is also known as an interference record, which is the total interference signal of a whole spectral band as a function of the optical path difference x. By subtracting the constant term:

$$\frac{1}{2}F(0) = 2\int_0^\infty E(\nu)d\nu \tag{2.13}$$

and using equation (2.12), we get:

$$I(x) = F(x) - \frac{1}{2}F(0) = 2\int_0^\infty E(\nu)\cos(2\pi\nu x)d\nu \tag{2.14}$$

where, $I(x)$ is an interferogram.

Now, suppose $E(\nu) = E(-\nu)$, then,

$$I(\mathrm{x}) = \int_{-\infty}^{\infty} E(\nu)\cos(2\pi\nu x)d\nu = \int_{-\infty}^{\infty} E(\nu)e^{j2\pi\nu x}d\nu$$

$$= F[\mathrm{E}(\nu)] \tag{2.15}$$

where F is the Fourier transform and we get a Fourier transform pair between $\mathrm{E}(\nu)$ and $I(\mathrm{x})$,

$$I(\mathrm{x}) = \int_{-\infty}^{\infty} E(\nu)e^{j2\pi\nu x}d\nu = F^{-1}[\mathrm{E}(\nu)] \tag{2.16}$$

and,

$$E(\nu) = \int_{-\infty}^{\infty} I(\mathrm{x})e^{-j2\pi\nu x}dx = F\ [I(\mathrm{x})] \tag{2.17}.$$

From the above equations, we can see that

$$I(\mathrm{x}) = F\{F^{-1}[I(\mathrm{x})]\} = F^{-1}\{F[I(\mathrm{x})]\} \tag{2.18}.$$

All the rules of Fourier transforms can be applied to the interferometer signal (which is a function of the optical path difference) and to the spectrum (as a function of wavenumber), as both these signals form a Fourier transform pair [YUE'07], [KAU'01].

The signal in the X-domain is usually the output of calculations in FTS. By taking the inverse Fourier transform of this signal, the most important information can be obtained which is in the ν- domain.

As the interferogram $I(\mathrm{x})$ is sampled at a set of discrete points with sampling interval $\Delta\,\mathrm{x}$, the spectrum cannot be calculated from the continuous equations (2.16,2.17):

$\mathrm{x}_j = j\Delta\,\mathrm{x}$ j=-N,-N+1,...,-1,0,1,...,N-1.

For $L = N\ \Delta\,\mathrm{x}$, data is collected from x= - L to x= L. Let the interferogram samples be $I\left(x_j\right) = I_j$ and applying discrete Fourier transform (DFT) we get:

$$E_L^{\Delta\mathrm{x}}(\nu) = \Delta\,\mathrm{x}\sum_{i=-N}^{N-1} I_j e^{-j2\pi\Delta\,\mathrm{x}\,\nu i} \tag{2.19}.$$

The continuous-truncated interferogram $I_L(\mathrm{x})$ is:

$$I_L(\mathrm{x}) = \prod_{2L}(\mathrm{x})\,\mathrm{I}(\mathrm{x}) \tag{2.20}$$

where, $\prod_{2L}$ is a boxcar function:

$$\prod_{2L}(\mathrm{x}) = 1 \qquad |\mathrm{x}| \le L,$$

$$= 0 \qquad |\mathrm{x}| > L.$$

Its spectrum can be given as:

$$E_L(\nu) = F^{-1}\{\prod_{2L}(\mathrm{x})I(\mathrm{x})\} = F^{-1}\{\prod_{2L}(\mathrm{x})\} * F^{-1}\{\mathrm{I}(\mathrm{x})\} = \mathrm{W}_L(\nu) * \mathrm{E}(\nu)$$

$$= \int_{-\infty}^{\infty} W_L(\mathrm{u})E(\nu - u)du \tag{2.21}$$

where,

$$\mathrm{W}_L(\nu) = F^{-1}\{\prod_{2L}(\mathrm{x})\} == \int_{-\infty}^{\infty} \prod_{2L}(\mathrm{x})e^{-j2\pi\nu x}dx = 2L\sin c(2\pi\nu L).$$

Not truncated, infinitely long sampled interferogram spectra can be given as:

$$E^{\Delta \mathrm{x}}(\nu) = \Delta \mathrm{x} \sum_{i=-\infty}^{\infty} I_j e^{-j2\pi\Delta \mathrm{x}\nu i} \tag{2.22}.$$

With the sampling interval, we get a periodic spectrum $E^{\Delta \mathrm{x}}(\nu)$ with the period $\frac{1}{\Delta \mathrm{x}}$ by the discrete sampling of an interferogram, i.e., $E^{\Delta \mathrm{x}}(\nu - \frac{k}{\Delta \mathrm{x}}) = E^{\Delta \mathrm{x}}(\nu)$ with integers k.

The spectrum of a non-truncated, sampled interferogram is:

$$E^{\Delta \mathrm{x}}(\nu) = \sum_{k=-\infty}^{\infty} E(\nu - \frac{k}{\Delta \mathrm{x}}) \tag{2.23}.$$

Considering both truncation and discrete sampling, we get the spectrum of a sampled, truncated interferogram:

$$E^{\Delta x}(\nu) = \sum_{k=-\infty}^{\infty} E_L(\nu - \frac{k}{\Delta x}) = E^{\Delta x}(\nu) = \sum_{k=-\infty}^{\infty} E_L(\nu) * \delta(\nu - \frac{k}{\Delta x})$$

$$= \sum_{k=-\infty}^{\infty} E(\nu) * \delta(\nu - \frac{k}{\Delta x}) * 2L\mathrm{sinc}(2\pi\nu L)$$

$$= \{\sum_{k=-\infty}^{\infty} 2L\mathrm{sinc}[(\nu - \frac{k}{\Delta x})L]\} * E(\nu) = W_L^{\Delta x}(\nu) * E(\nu) \quad (2.24)$$

where,

$$W_L^{\Delta x}(\nu) = \sum_{k=-\infty}^{\infty} 2L\mathrm{sinc}[2\pi(\nu - \frac{k}{\Delta x})L].$$

$W_L^{\Delta x}(\nu)$ is called as the instrumental function of a Fourier transform spectrometer.

The monochromatic spectrum of spectral lines at wavenumber $+\nu_0$ and $-\nu_0$ has a spectrum:

$$E(\nu) = \delta(\nu + \nu_0) + \delta(\nu - \nu_0) \quad (2.25).$$

The interferogram is its corresponding signal:

$$I(x) = F[E(\nu)] = e^{j2\pi\nu_0 x} + e^{-j2\pi\nu_0 x} = 2\cos(2\pi\nu_0 x) \quad (2.26).$$

For truncated interferograms, i.e., for a signal recorded from x= $-L$ to x= L, the spectrum is:

$$E_L(\nu) = W_L(\nu) * [\delta(\nu + \nu_0) + \delta(\nu - \nu_0)]$$

$$= W_L\,\delta(\nu + \nu_0) + W_L\,\delta(\nu - \nu_0)$$

$$= 2L\mathrm{sinc}[2\pi(\nu + \nu_0)L] + 2L\mathrm{sinc}[2\pi(\nu - \nu_0)L] \quad (2.27).$$

The frequency of monochromatic light can be calculated as:

$$\mathrm{f} = \frac{\omega_0}{2\pi\nu_0} c \tag{2.28}$$

where ω_0 is the frequency position of spectrum lines which depends on the frequency of light and the moving mirror speed. The accuracy of the measurement of an optical frequency is proportional to the stability of speed of the moving mirror.

If the maximum optical path difference of the interferometer is L, then the theoretical resolution of a spectrum is the full width at half maximum (FWHM) of the sinc function [YUE'07], [KAU'01]:

$$\delta\nu \approx \frac{1.207}{2L} \tag{2.29}.$$

The critical sampling interval of an interferometric signal is the inverse of the Nyquist frequency:

$$(\Delta \mathrm{x})_{Nyquist} = \frac{1}{2\nu_{\max}} \tag{2.30}$$

where $\nu_{\max}$ is the maximum wavenumber of the spectral band. The spectrum $E_L^{\Delta \mathrm{x}}(\nu)$ calculated using this optimal sampling interval contains no free regions, whereas for $\Delta \mathrm{x} > \frac{1}{2\nu_{\max}}$, i.e., for larger sampling intervals than the maximum one, aliasing in the spectrum occurs due to the different spectral orders (different *l* and *k*) which distorts the spectrum $E_L^{\Delta \mathrm{x}}(\nu)$.

The optical frequency of a 633nm laser is $f_{633\mathrm{nm}}$. So the Nyquist interval sampling frequency is:

$$\omega_S \geq \frac{2\pi\nu_0 f_S}{c} \tag{2.31}.$$

Using equations (2.28) and (2.31):

$$f_s \leq Z \times f_{633nm} \tag{2.32}$$

where f_s is the optical spectrum width, and Z is some integer. Usually the value of Z =8 is used, which means that the optical spectrum width is approximately 8 times the frequency of the reference laser [YUE'07].

Windowing is another big factor that plays a part in estimating a spectrum. A window function can be used in equation (2.20) instead of the truncation function to reduce the sidelobes. This window function is unity at x=0 and approaches zero for large values of |x|. This method is also known as apodization (or tapering) [KAU'01]. The spectrum from equation (2.21) can be written as:

$$E_A(\nu) = F^{-1}[\mathrm{A(x)}I(\mathrm{x})]\} = F^{-1}[\mathrm{A(x)}] * \mathrm{E}(\nu) = W_A(\nu) * \mathrm{E}(\nu) \tag{2.33}$$

where $\mathrm{A(x)}$ is the apodization function, e.g. a triangular function:

$$\mathrm{A(x)} = 1 - \frac{|\,\mathrm{x}\,|}{L} \qquad |\,\mathrm{x}\,| \leq L\,, \qquad\qquad \mathrm{A(x)} = 0 \qquad |\,\mathrm{x}\,| > L\,.$$

Its FWHM is L. The inverse Fourier transform of the triangular function is:

$$W_A(\nu) = \mathrm{W}_{A_L}(\nu) = \mathrm{L}\,\mathrm{sinc}^2(\pi\nu L)\,. \tag{2.34}$$

Chapter 3 Non-Parametric Power Spectrum Estimation Techniques

3.1 Basics of Power spectrum density

The problem of finding a power spectrum density is usually associated with wide sense stationary signals (WSS). Due to random fluctuations in signals, it is necessary to deal with the average characteristics of random signals. The Fourier transform of an autocorrelation sequence gives the power spectrum density. There are a couple of drawbacks of this method. First, the amount of data is limited and may be very short. This may happen due to characteristics of the process data collection. A second problem is the amount of noise which corrupts the recorded data [PRO'96], [STO'05]. Therefore estimation of a power spectrum density problem involves a finite number of noisy measurements of a signal x(n).

The power spectrum density estimation problem involves two approaches. One is non-parametric methods while the other is parametric methods. Non-parametric methods conceptually require to calculate the autocorrelation sequence from a given data and the Fourier transform of this estimated autocorrelation sequence gives the power spectrum. Parametric methods involve a modeling of the process to estimate the power spectrum [STO'05], [ZAK'05]. This chapter focuses on non-parametric methods, while the next chapter will focus on parametric methods.

As stated earlier, a finite data record has an impact on the power spectrum estimation quality. The longer the data record, the better the power spectrum estimate is obtained for statistically stationary signals. In nonstationary statistical signals, the length of a data record is determined by time variations in signal statistics [ZAK'05].

Sampling continuous time signal $x_a(\mathrm{t})$ at sampling rate F_s gives the sequence x(n). If $x_a(\mathrm{t})$ is a finite energy signal equation as per (3.1) then its Fourier transform exists and is given as in equation (3.2):

$$E = \int_{-\infty}^{\infty} | x_a(\mathrm{t}) |^2 \, dt < \infty \tag{3.1}$$

$$X_a(\mathrm{F}) = \int_{-\infty}^{\infty} x_a(\mathrm{t}) e^{-j2\pi Ft} dt \tag{3.2}.$$

Parseval's theorem gives:

$$E = \int_{-\infty}^{\infty} | x_a(\mathrm{t}) |^2 \, dt = \int_{-\infty}^{\infty} | \mathrm{X}_a(\mathrm{F}) |^2 \, dF \tag{3.3}.$$

$|X_a(F)|^2$ is the energy density spectrum of the signal, as this term represents the signal energy distribution as a function of frequency:

$$S_{xx}(F) = |X_a(F)|^2 \tag{3.4}$$

The total area under $S_{xx}(F)$ provides the total energy in the signal. $S_{xx}(F)$ is the Fourier transform of the autocorrelation function $R_{xx}(\tau)$ of the finite energy signal:

$$R_{xx}(\tau) = \int_{-\infty}^{\infty} x_a^*(t)\, x_a(t+\tau)\, dt \tag{3.5}$$

$$S_{xx}(F) = \int_{-\infty}^{\infty} R_{xx}(\tau)\, e^{-j2\pi F\tau}\, d\tau = |X_a(F)|^2 \tag{3.6}$$

Equation (3.6) shows that $S_{xx}(F)$ and $R_{xx}(\tau)$ are a Fourier transform pair.

To avoid the aliasing problem in the power spectrum density of signal $x_a(t)$, the signal is prefiltered and its bandwidth is B Hertz which gives a sampling frequency F_s>2B. This sampled sequence $x(n)$ has a Fourier transform:

$$X(f) = \sum_{n=-\infty}^{\infty} x(n)\, e^{-j2\pi fn} \tag{3.7}$$

The autocorrelation of the sampled signal can be given as:

$$\gamma_{xx}(k) = \sum_{n=-\infty}^{\infty} x^*(n)\, x(n+k) \tag{3.8}$$

and its Fourier transform is:

$$S_{xx}(f) = \sum_{k=-\infty}^{\infty} \gamma_{xx}(k)\, e^{-j2\pi kf} \tag{3.9}$$

This shows that the power spectrum density is obtained by taking the Fourier transform of the autocorrelation sequence of sampled signal $x(n)$ [PRO'96].

Limiting the duration of $x(n)$ to N-points, $0 \leq n \leq N\text{-}1$, is similar to applying a rectangular window to the signal:

$$\bar{x}(n) = x(n)\, w(n) = x(n) \qquad 0 \leq n \leq N\text{-}1 \qquad (3.10).$$

$$= 0 \qquad \text{otherwise}$$

Multiplication of two sequences is equal to a convolution of their spectra, i.e.:

$$\overline{X}(f) = X(f) * W(f) = \int_{-1/2}^{1/2} X(\alpha)\, W(f-\alpha)\, d\alpha \qquad (3.11).$$

The spectrum $\overline{X}(f)$ is smoothen due to the convolution of the window function W(f) with $X(f)$, with a condition that the spectrum of W(f) is narrower than $X(f)$, i.e., w(n) should be sufficiently long. Having W(f) narrower than $X(f)$ doesn't help in reducing the sidelobes in the spectrum $\overline{X}(f)$. This problem of leakage can be reduced by using a window with smooth time domain cutoff, unlike rectangular windows. But it results in increased loss of frequency resolution in $X(f)$, which is undesirable to distinguish the closely spaced signal components in the spectrum. An approximation of the desired spectrum of the sequence $x(n)$ gives the power spectrum density:

$$S_{\bar{x}\bar{x}}(f) = |\overline{X}(f)|^2 = \left| \sum_{n=0}^{N-1} \bar{x}(n)\, e^{-j2\pi fn} \right|^2 \qquad (3.12).$$

Using the DFT, the spectrum can be calculated at N frequency points by:

$$\overline{X}(k) = \sum_{n=0}^{N-1} \bar{x}(n)\, e^{-j2\pi kfN} \qquad (3.13).$$

Thus,

$$S_{\bar{x}\bar{x}}(f)\big|_{f=k/N} = S_{\bar{x}\bar{x}}\left(\frac{k}{N}\right) = \sum_{n=0}^{N-1} \bar{x}(n)\, e^{-j2\pi kfN} \qquad (3.14)$$

which gives a distorted version of true spectrum,

$$S_{xx}(\frac{k}{N}) = | \sum_{n=0}^{N-1} x(n) e^{-j2\pi kfn/N} |^2 \quad (3.15).$$

3.2 Basics of the Periodogram

Stationary random processes have finite power and are estimated by power spectrum density, unlike finite energy signals which possess a Fourier transform[PRO'96], [BEL'01]. The autocorrelation function of a stationary random process x(t) is:

$$\gamma_{xx}(\tau) = E[x^*(t)\, x(t+\tau)] \quad (3.16)$$

where a statistical average is represented by E[ ].

The Fourier transform of the autocorrelation function provides the power spectrum density of the stationary random process by Wiener theorem:

$$\Gamma_{xx}(F) = \int_{-\infty}^{\infty} \gamma_{xx}(\tau) e^{-j2\pi F\tau}\, d\tau \quad (3.17).$$

In practice, using a Fourier transform to calculate $\Gamma_{xx}(F)$ is not possible as the true autocorrelation function $\gamma_{xx}(\tau)$ is unknown. But a single realization of the random process can be used to calculate a time average autocorrelation function:

$$R_{xx}(\tau) = \frac{1}{2T_0} \int_{-T_0}^{T_0} x^*(t)\, x(t+\tau) dt \quad (3.18),$$

where $2\ T_0$ is the observation interval. For stationary random processes ergodic in mean and autocorrelation:

$$\gamma_{xx}(\tau) = \lim_{T_0 \to \infty} R_{xx}(\tau) \quad (3.19).$$

This shows that the time average autocorrelation $R_{xx}(\tau)$ can be used as an estimate of the statistical autocorrelation function $\gamma_{xx}(\tau)$. The power spectrum density $P_{xx}(F)$ can be obtained by taking the Fourier transform of $R_{xx}(\tau)$:

$$P_{xx}(\mathrm{F}) = \int_{-T_0}^{T_0} R_{xx}(\tau)\, \mathrm{e}^{-j2\pi F\tau}\, d\tau$$

$$= \frac{1}{2T_0} \int_{-T_0}^{T_0} [\int_{-T_0}^{T_0} \mathrm{x}^*(\mathrm{t})\, \mathrm{x}(\mathrm{t}+\tau) dt]\, \mathrm{e}^{-j2\pi F\tau}\, d\tau$$

$$= \frac{1}{2T_0} | \int_{-T_0}^{T_0} x(\mathrm{t})\, \mathrm{e}^{-j2\pi Ft}\, dt\, |^2 \qquad (3.20).$$

The expected value of $P_{xx}(\mathrm{F})$ gives the true power spectrum density:

$$\Gamma_{xx}(\mathrm{F}) = \lim_{T_0 \to \infty} E[P_{xx}(\mathrm{F})]$$

$$= \lim_{T_0 \to \infty} E[\frac{1}{2T_0} | \int_{-T_0}^{T_0} x(\mathrm{t})\, \mathrm{e}^{-j2\pi Ft}\, dt\, |^2] \qquad (3.21).$$

$P_{xx}(\mathrm{F})$ can be computed by two methods which are 1) directly using equation (3.20) and 2) indirectly by calculating $R_{xx}(\tau)$ and then taking its Fourier transform [HAY'97].

The autocorrelation sequence for finite duration data $x(\mathrm{n})$, $0 \le \mathrm{n} \le N$ -1, for a single realization of a random process is:

$$\gamma'_{xx}(\mathrm{m}) = \frac{1}{N-m} \sum_{n=0}^{N-m-1} x^*(\mathrm{n})\, \mathrm{x}(\mathrm{n}+m) \qquad m = 0,1,..., N-1 \qquad (3.22)$$

$$\gamma'_{xx}(\mathrm{m}) = \frac{1}{N-|m|} \sum_{n=|m|}^{N-1} x^*(\mathrm{n})\, \mathrm{x}(\mathrm{n}+m) \qquad m = -1,-2,...,-N+1 \qquad (3.23).$$

Then the Fourier transform is:

$$P'_{xx}(\mathrm{F}) = \sum_{m=-N+1}^{N-1} \gamma'_{xx}(\mathrm{m})\, \mathrm{e}^{-j2\pi Fm} \qquad (3.24).$$

For large lag values m, estimates of $\gamma'_{xx}(\mathrm{m})$ from equations (3.22,3.23) have a large variance for

$m \to N$, as few data points are used for the estimation for large lags. The following equations can be used instead of equations (3.22,3.23):

$$\gamma_{xx}(\mathrm{m}) = \frac{1}{N} \sum_{n=0}^{N-m-1} \mathrm{x}^{*}(\mathrm{n})\,\mathrm{x}(\mathrm{n}+m) \qquad 0 \le m \le N\text{-}1 \tag{3.25}$$

$$\gamma_{xx}(\mathrm{m}) = \frac{1}{N} \sum_{n=|\mathrm{m}|}^{N-1} \mathrm{x}^{*}(\mathrm{n})\,\mathrm{x}(\mathrm{n}+m) \qquad m = -1,-2,\ldots,-N+1 \tag{3.26}$$

Using the above biased $\gamma_{xx}(\mathrm{m})$ estimates, estimates of the power spectrum density can be obtained:

$$P_{xx}(\mathrm{f}) = \sum_{m=-N+1}^{N-1} \gamma_{xx}(\mathrm{m})\,\mathrm{e}^{-j2\pi fm} \tag{3.27}$$

By substituting $\gamma_{xx}(\mathrm{m})$ from equations (3.25,3.26), estimates of the power spectrum density $P_{xx}(\mathrm{f})$ can be obtained:

$$P_{xx}(\mathrm{f}) = \frac{1}{N} \left| \sum_{n=0}^{N-1} \mathrm{x}(\mathrm{n})\,\mathrm{e}^{-j2\pi fn} \right|^2 = \frac{1}{N} |\, X(\mathrm{f}) \,|^2 \tag{3.28}$$

This is a power spectrum density which is famously known as the periodogram, which was invented by Schuster (1898) to detect and measure 'hidden periodicities' in data. But the periodogram is not a consistent estimate of the true power spectrum density, as the statistical variance of the periodogram estimate does not decay with the increasing values of N [HAY'97], [MAN'05].

For N data points, an N-points DFT can be used to compute samples of the periodogram:

$$P_{xx}\left(\frac{k}{N}\right) = \frac{1}{N} \left| \sum_{n=0}^{N-1} \mathrm{x}(\mathrm{n})\,\mathrm{e}^{-j2\pi nk/\mathrm{N}} \right|^2 \qquad \mathrm{k} = 0,1,\ldots,\ N\text{-}1 \tag{3.29}$$

for frequencies at $f_k = \frac{k}{N}$.

This sampling of a spectrum is not necessarily a good visual representation of a continuous spectrum estimate $P_{xx}(\mathrm{f})$. This can be improved by adding additional frequencies, i.e., by increasing the sequence

length with zero padding and evaluating $P_{xx}(\frac{k}{N})$. So we then get an L-point data sequence and an L-point DFT given as:

$$P_{xx}(\frac{k}{L}) = \frac{1}{N}|\sum_{n=0}^{N-1} \mathrm{x(n)}\, \mathrm{e}^{-j2\pi nk/\mathrm{L}}|^2 \qquad \mathrm{k} = 0,1,..., L\text{-}1 \qquad (3.30).$$

Zero padding doesn't improve the physical frequency resolution of the spectrum estimate, instead it helps to interpolate the values of the measured spectrum at more frequencies. The original data record length N (or window length) still accounts for the true frequency resolution of the spectral estimate $P_{xx}(\mathrm{f})$ [PRO'96].

3.3 Other Non-parametric Power Spectrum Estimation Techniques

The periodogram suffers from not being a statistically consistent estimate of the power spectrum density [CAS'11]. Other non-parametric methods have been developed to overcome this problem. Like the periodogram, these methods don't use any assumption on how the data was generated, hence they are known as non-parametric methods. Consistent estimates of power spectrum density are obtained by smoothing or averaging operations on the autocorrelation or the periodogram. Non-parametric methods decrease the variance in the estimates of the power spectrum (making it a consistent estimate) but at the cost of reduced frequency resolution. A number of modifications on the periodogram method have been developed to improve its statistical properties [STO'05], [MAN'05]. Three popular methods are the Bartlett method, the Welch method and the Blackman and Tukey method.

3.3.1 Barlett method

The Barlett method is one of the periodogram averaging method which produces consistent estimates of the power spectrum with less variance than the periodogram. In this method, the N-point sequence is first divided into K non-overlapping data segments each with a segment length M [HAY'97]:

$$x_i(\mathrm{n}) = \mathrm{x(n+iM)}$$

where, i=0,1,...,K-1

n =0,1,...,M-1

A periodogram is computed for each data segment:

$$P_{xx}^{(i)}(f) = \frac{1}{M} \left| \sum_{n=0}^{M-1} x_i(n) e^{-j2\pi fn} \right|^2 \tag{3.31}$$

where i=0,1,...,K-1.

At the end, the Bartlett power spectrum estimate is calculated by averaging the periodograms from each of the K data segments:

$$P_{xx}^{B}(f) = \frac{1}{K} \sum_{i=0}^{K-1} P_{xx}^{(i)}(f) \tag{3.32}.$$

The statistical properties of the Bartlett method can be calculated as follows. Its mean value is given as:

$$E[P_{xx}^{B}(f)] = \frac{1}{K} \sum_{i=0}^{K-1} E[P_{xx}^{(i)}(f)] = E[P_{xx}^{(i)}(f)] \tag{3.33}.$$

The expected value for a single periodogram is:

$$E[P_{xx}^{(i)}(f)] = \sum_{m=-[M-1]}^{M-1} \left(1 - \frac{|m|}{M}\right) \gamma_{xx}(m) e^{-j2\pi fm}$$

$$= \frac{1}{M} \int_{-1/2}^{1/2} \Gamma_{xx}(\alpha) \left(\frac{\sin \pi (f-\alpha) M}{\sin \pi (f-\alpha)} \right)^2 d\alpha \tag{3.34}.$$

The frequency characteristics of the Bartlett (triangular) window is:

$$W_B(f) = \frac{1}{M} \left(\frac{\sin \pi fM}{\sin \pi f} \right)^2 \tag{3.35}$$

where

$$w_B(n) = 1 - \frac{|m|}{M}, \qquad |m| \le M-1$$

$$= 0 \qquad \text{otherwise.}$$

From the above equation, it can be seen that the frequency characteristic of the Bartlett window gets convolved with the true spectrum. The spectral width of the window is increased by a factor of K as the data length is divided from -points to M= N /K points, which results in a reduction in frequency resolution by a factor of K.

On the other hand, the variance is reduced by this method compared to the variance of the periodogram, with the following result:

$$\mathrm{var}[P_{xx}^{B}(\mathrm{f})] = \frac{1}{K^2}\sum_{i=0}^{K-1}\mathrm{var}[P_{xx}^{(\mathrm{i})}(\mathrm{f})] = \frac{1}{K}\mathrm{var}[P_{xx}^{(\mathrm{i})}(\mathrm{f})] \qquad (3.36).$$

This shows that by using the Bartlett power spectrum estimate the variance is reduced by a factor of K [HAY'97], [PRO'96].

3.3.2 Welch Method

The Welch method is similar to the Bartlett method with two modifications. In this method, the data segments are overlapped [WEL'67]:

$$x_i(\mathrm{n}) = \mathrm{x}(\mathrm{n}+\mathrm{iD})$$

where,

n=0,1,...,M-1

i=0,1,...,L-1

and the i th sequence starts from iD (window shift is D).

The segments do not overlap if D=M and if the number of data segments L is equal to the number of data segments K in the Bartlett method. Successive data segments overlap by 50% if D=M/2 , and L=2K data segments are then formed.

Before computing the periodogram, the data segments are windowed. This is the second modification done from the Bartlett method [STO'05]. Now the modified periodogram is:

$$\overline{P}_{xx}^{(\mathrm{i})} = \frac{1}{MU}\left|\sum_{n=0}^{M-1} x_{(\mathrm{i})}(\mathrm{n})\,\mathrm{w}(\mathrm{n})\,\mathrm{e}^{-j2\pi fn}\right|^2 \qquad \mathrm{i}=0,1,...,\mathrm{L}-1 \qquad (3.37)$$

where U is a normalization factor for the power in the window:

$$U = \frac{1}{M}\sum_{n=0}^{M-1} w^2(\mathrm{n}) \tag{3.38}$$

By taking the average of all the modified periodograms, the Welch power spectrum estimate is obtained:

$$P_{xx}^{W}(\mathrm{f}) = \frac{1}{L}\sum_{i=0}^{L-1}\overline{P_{xx}^{(i)}}(\mathrm{f}) \tag{3.39}$$

Its statistical properties are easy to find. It's mean value is:

$$E[P_{xx}^{W}(\mathrm{f})] = \frac{1}{L}\sum_{i=0}^{L-1} E[\overline{P_{xx}^{(i)}}(\mathrm{f})]$$

$$= E[\overline{P_{xx}^{(i)}}(\mathrm{f})] \tag{3.40}$$

The expected value of the modified periodogram is:

$$E[\overline{P}_{xx}^{(\mathrm{i})}] = \frac{1}{MU}\sum_{m=0}^{M-1}\sum_{n=0}^{M-1} E[x_{(\mathrm{i})}(\mathrm{n})x_{(\mathrm{i})}{}^{*}(\mathrm{m})]\,\mathrm{w}(\mathrm{n})\,\mathrm{w}(\mathrm{m})\,\mathrm{e}^{-j2\pi f(n-m)}$$

$$= \frac{1}{MU}\sum_{m=0}^{M-1}\sum_{n=0}^{M-1}\gamma_{xx}(\mathrm{n}-\mathrm{m})\,\mathrm{w}(\mathrm{n})\,\mathrm{w}(\mathrm{m})\,\mathrm{e}^{-j2\pi f(n-m)} \tag{3.41}$$

As $\gamma_{xx}(\mathrm{n}) = \int_{-1/2}^{1/2}\Gamma_{xx}(\alpha)\,\mathrm{e}^{j2\pi\alpha n}\,d\alpha$, by substituting the equation into (3.41), we get:

$$E[\overline{P}_{xx}^{(\mathrm{i})}] = \frac{1}{MU}\int_{-1/2}^{1/2}\Gamma_{xx}(\alpha)[\sum_{m=0}^{M-1}\sum_{n=0}^{M-1}\mathrm{w}(\mathrm{n})\,\mathrm{w}(\mathrm{m})\,\mathrm{e}^{-j2\pi(f-\alpha)(n-m)}]d\alpha$$

$$= \int_{-1/2}^{1/2}\Gamma_{xx}(\alpha)\,\mathrm{W}(\mathrm{f}-\mathrm{a})d\alpha \tag{3.42}$$

where

$$W(\mathrm{f}) = \frac{1}{MU} \left| \sum_{n=0}^{M-1} w(\mathrm{n})\, \mathrm{e}^{-j2\pi fn} \right|^2 .$$

The variance of the Welch estimate can be given as:

$$\mathrm{var}[P_{xx}^{W}(\mathrm{f})] = \frac{1}{L^2} \sum_{j=0}^{L-1} \sum_{i=0}^{L-1} E[\overline{P_{xx}^{(i)}}(\mathrm{f}) \overline{P_{xx}^{(\mathrm{j})}}(\mathrm{f})] - \{\mathrm{E}[P_{xx}^{W}(\mathrm{f})]\}^2 \qquad (3.43).$$

The variance of the Welch power spectrum estimate with a triangular window when there is an overlap of 50% between successive data segments is:

$$\mathrm{var}[P_{xx}^{W}(\mathrm{f})] \approx \frac{9}{8L} \Gamma_{xx}^{2}(\mathrm{f}) \qquad (3.44).$$

The variance will be different for different windows used [PRO'96]. Overlapping of data segment may also be changed in order to change different characteristics of this estimate.

3.3.3 Blackman and Tukey Method

The Bartlett and Welch methods make use of averaging periodograms and modified periodograms, respectively, to decrease the variance of the periodogram. Statistical variability can be decreased by using another type of method which is periodogram smoothing [PRO'96].

In order to understand the working of periodogram smoothing for reducing the variance of the periodogram, we know that the periodogram is calculated by taking the Fourier transform of a consistent estimate of the autocorrelation sequence. For any finite data record of length N, the variance of the autocorrelation $\gamma_{xx}(\mathrm{m})$ will be larger for values of m closer to N. So these estimates will be very noisy for $|\mathrm{m}| \approx N$ for any large values of N, as a small number of data points are used for these estimates. Therefore, a window can be applied to the $\gamma_{xx}(\mathrm{m})$ estimate to reduce the influence of these noisy estimates when computing a periodogram [HAY'97], [PRO'96].

The Blackman and Tukey method works in the following way [PRO'96]. First the autocorrelation sequence is windowed and then the power spectrum estimates are obtained by taking its Fourier transform:

$$\mathrm{P}_{xx}^{BT}(\mathrm{f}) = \sum_{m=-(\mathrm{M}-1)}^{M-1} \gamma_{xx}(\mathrm{m})\, \mathrm{w}(\mathrm{m})\, \mathrm{e}^{-j2\pi fm} \qquad (3.45)$$

where the window function w(m) length is 2M-1, i.e., it is zero for $|\mathrm{m}| \geq \mathrm{M}$.

The frequency domain equivalent expression of equation (3.45) is:

$$\mathrm{P}_{xx}^{BT}(\mathrm{f}) = \int_{-1/2}^{1/2} P_{xx}(\alpha)\, \mathrm{W}(\mathrm{f}-\alpha)\, d\alpha \tag{3.46}$$

which is obtained after extending the limits of equation (3.45) to $(-\infty, \infty)$. From the above equation it can be seen that windowing the autocorrelation sequences smoothens the periodogram estimate. Though variance is reduced by using this method, it also reduces the frequency resolution of the estimate [PRO'96].

For the power spectrum estimate to be real, it is important that the window sequence about m=0 must be symmetric, such that it spectrum is real. Also, the window spectrum should be nonnegative:

$W(\mathrm{f}) \geq 0 \qquad\qquad |f| \leq 1/2$.

With the above conditions, $P_{xx}^{BT}(\mathrm{f}) \geq 0$ for $|f| \leq 1/2$.

The expected value of the Blackman Tukey power spectrum estimate is:

$$E[P_{xx}^{BT}(\mathrm{f})] = \int_{-1/2}^{1/2} E[\mathrm{P}_{xx}(\alpha)]W(\mathrm{f}-\alpha)\, d\alpha \tag{3.47}.$$

Since

$$E[\mathrm{P}_{xx}(\alpha)] = \int_{-1/2}^{1/2} \Gamma_{xx}(\theta)\, \mathrm{W}_B(\alpha-\theta)\, d\theta \tag{3.48},$$

putting equation (3.48) into equation (3.47), we get:

$$E[\mathrm{P}_{xx}^{BT}(\mathrm{f})] = \int_{-1/2}^{1/2}\int_{-1/2}^{1/2} \Gamma_{xx}(\theta)\, \mathrm{W}_B(\alpha-\theta)\, \mathrm{W}(\mathrm{f}-\alpha)\, d\alpha\, d\theta \tag{3.49}.$$

The expected value in the time domain can be given as:

$$E[\mathrm{P}_{xx}^{BT}(\mathrm{f})] = \sum_{m=-(\mathrm{M}-1)}^{M-1} E[\gamma_{xx}(\mathrm{m})]w(\mathrm{m})\, \mathrm{e}^{-j2\pi fm}$$

$$= \sum_{m=-(M-1)}^{M-1} \gamma_{xx}(\mathrm{m}) w(\mathrm{m})\, \mathrm{w}_B(\mathrm{m})\, \mathrm{e}^{-j2\pi fm} \qquad (3.50),$$

where

$$\mathrm{w}_B(\mathrm{m}) = 1 - \frac{|m|}{N}, \qquad |m| < \mathrm{N}$$

$$= 0, \qquad \text{otherwise.}$$

For improved smoothing of the periodogram, the window length w(n) should be shorter than $\mathrm{w}_B(\mathrm{m})$, i.e., M<<N.

The variance of the Blackman Tukey estimate is:

$$\mathrm{var}[\mathrm{P}_{xx}^{BT}(\mathrm{f})] = E\{[\mathrm{P}_{xx}^{BT}(\mathrm{f})^2]\} - \{E[\mathrm{P}_{xx}^{BT}(\mathrm{f})]\}^2$$

$$\approx \frac{1}{N} \int_{-1/2}^{1/2} \Gamma_{xx}(\alpha)\, \mathrm{W}(\mathrm{f}-\alpha)[\Gamma_{xx}(-\alpha)\, \mathrm{W}(\mathrm{f}+\alpha) + \Gamma_{xx}(\alpha)\, \mathrm{W}(\mathrm{f}-\alpha)]d\alpha$$

$$\approx \frac{1}{N} \int_{-1/2}^{1/2} \Gamma_{xx}^2(\alpha)\, \mathrm{W}^2(\mathrm{f}-\alpha) d\alpha \qquad (3.51).$$

To summarize all the non-parametric methods discussed in this section, their performance characteristics are as given in the Table 3.1.

Table 3.1: Performance characteristics of non-parametric PSD estimation methods

Method	PSD	Mean	Variance
Bartlett	$P_{xx}^B(\mathrm{f}) = \frac{1}{K}\sum_{i=0}^{K-1} P_{xx}^{(\mathrm{i})}(\mathrm{f})$	$E[P_{xx}^B(\mathrm{f})] = \frac{1}{K}\sum_{i=0}^{K-1} E[P_{xx}^{(\mathrm{i})}(\mathrm{f})] = \mathrm{E}[P_{xx}^{(\mathrm{i})}(\mathrm{f})]$	$\mathrm{var}[P_{xx}^B(\mathrm{f})] = \frac{1}{K^2}\sum_{i=0}^{K-1} \mathrm{var}[P_{xx}^{(\mathrm{i})}(\mathrm{f})] = \frac{1}{K}\mathrm{var}[P_{xx}^{(\mathrm{i})}(\mathrm{f})]$
Welch	$P_{xx}^W(\mathrm{f}) = \frac{1}{L}\sum_{i=0}^{L-1} \overline{P_{xx}^{(i)}}(\mathrm{f})$	$E[P_{xx}^W(\mathrm{f})] = \frac{1}{L}\sum_{i=0}^{L-1} E[\overline{P_{xx}^{(i)}}(\mathrm{f})]$	$\mathrm{var}[\mathrm{P}_{xx}^W(\mathrm{f})] \approx \frac{1}{L}\Gamma_{xx}^2(\mathrm{f})$
Blackman-Tukey	$\mathrm{P}_{xx}^{BT}(\mathrm{f}) = \sum_{m=-(M-1)}^{M-1} \gamma_{xx}(\mathrm{m})\, \mathrm{w}(\mathrm{m})\, \mathrm{e}^{-j2\pi fm}$	$\mathrm{E}[\mathrm{P}_{xx}^{BT}(\mathrm{f})] \approx \frac{1}{N}\int_{-1/2}^{1/2} \Gamma_{xx}(\theta)\, \mathrm{W}(\mathrm{f}-\theta) d\theta$	$\mathrm{var}[\mathrm{P}_{xx}^{BT}(\mathrm{f})] \approx \frac{1}{N}\int_{-1/2}^{1/2} \Gamma_{xx}^2(\alpha)\, \mathrm{W}^2(\mathrm{f}-\alpha) d\alpha$

Let the data length be N with a specified resolution Δf and the use of a radix-2 FFT algorithm is assumed. The number of complex multiplication required to measure the estimate of the PSD for the non-parametric methods are given in Table 3.2 [PRO'96].

Table 3.2: Computational complexity of non-parametric method

Method	FFT length	Number of Computations	Number of FFTs
Bartlett	$M = 0.9/\Delta f$	$\frac{N}{2}\log_2(0.9/\Delta f)$	$\frac{N}{M} = 1.11N\Delta f$
Welch	$M = 1.28/\Delta f$	$N\log_2(5.12/\Delta f)$	$\frac{2N}{M} = 1.56N\Delta f$
Blackman-Tukey	$2M = 1.28/\Delta f$	$N\log_2(1.28/\Delta f)$	$\frac{N}{M}$

3.4 FFT and zoom FFT

At the very core of the non-parametric PSD estimation methods is the computation of a DFT using an efficient FFT algorithm. This section will discuss the concepts of the FFT and the zoom-FFT, which are critical for real-time implementations of non-parametric PSD estimation methods, such as the one required in this project.

A fast implementation of the DFT is through a fast Fourier transform (FFT). In this approach the DFT is divided into smaller, simpler DFTs, and the final DFT is just a combination of these smaller DFTs. This approach is known as the divide and conquer method [ORF]. In radix-2 FFTs, the dimension of the DFTs is successively divided into half till it is unity. The condition for this is that the initial dimension N has to be a power of two (or zero padding can be used to increase the length to a power of two):

$$N = 2^B$$

and

$$B = \log_2 N \text{ is an integer} \qquad (3.52).$$

This method was proposed by Cooley-Tukey. The N -point DFT is solved by dividing it into the smaller two (N /2) points DFTs. Each is these DFTs is then divided into two (N /4) point DFTs and so on.

The total cost of rebuilding the full N -point DFT from two (N /2) DFTs at a cost of (N /2)^2 multiplications is:

$$2\left(\frac{N}{2}\right)^2 + \frac{N}{2} = \frac{N^2}{2} + \frac{N}{2} \approx \frac{N^2}{2} \tag{3.53}.$$

This saves approximately 50% of the computations over an N -point DFT which costs N^2. If we start with (N /(2^m))-points DFTs and do m successive merging steps, the final N -point DFT will cost:

$$\frac{N^2}{2^m} + \frac{N}{2}m \tag{3.54}.$$

The initial (N /(2^m))-points DFTs cost $\frac{N^2}{2^m}$, which is the first term in above equation. So total cost will be:

$$2^m\left(\frac{N}{2^m}\right)^2 = \frac{N^2}{2^m} \tag{3.55}.$$

For m=B subdivision stages, the final dimension is:

$$\frac{N}{2^m} = \frac{N}{2^B} = 1 \tag{3.56},$$

i.e., the 1-point DFT of a 1-point signal, which is itself and requires no computation. This shows that the total computation cost of the subdividing/merging process for m= $B = \log_2 N$ stages is:

$$\frac{1}{2}NB = \frac{1}{2}N\log_2 N \tag{3.57}.$$

Using this discussion about the FFT, the decimation in time radix-2 FFT algorithm can be explained. For a N -length sequence $x(\mathrm{n})$, n =0,1,..., N -1, the N -point DFT $X(\mathrm{k}) = \mathrm{X}(\mathrm{w}_k)$ is:

$$X(\mathrm{k}) = \sum_{n=0}^{N-1} W_N^{kn}\, x(\mathrm{n}) \qquad \mathrm{k}=0,1,\ldots,\ -1 \tag{3.58}.$$

Even indexed and odd indexed terms from the above equation for range $0 \le n \le N-1$ can be grouped:

$$X(\mathrm{k}) = \sum_{n=0}^{N/2-1} W_N^{k(2n)} x(2\mathrm{n}) + \sum_{n=0}^{N/2-1} W_N^{k(2n+1)} x(2\mathrm{n}+1) \qquad (3.59).$$

Equation (3.59) gives two N /2-length sequences:

$$\mathrm{g(n)=x(2n)} \quad \text{and} \quad \mathrm{h(n)=x(2n+1)} \qquad \mathrm{n=0,1,...,}\ N/2\text{-}1 \qquad (3.60).$$

The DFTs of these two (N /2) points are:

$$\mathrm{G(k)} = \sum_{n=0}^{N/2-1} W_{N/2}^{kn}\, \mathrm{g(n)}$$

$$\mathrm{H(k)} = \sum_{n=0}^{N/2-1} W_{N/2}^{kn}\, \mathrm{h(n)} \qquad \mathrm{k=0,1,...,}\ N/2\text{-}1 \qquad (3.61).$$

Defining the twiddle factors $W_N = \mathrm{e}^{-j2\pi/\mathrm{N}}$, $W_{N/2}$ and W_N are related as:

$$W_{N/2} = \mathrm{e}^{-j2\pi/(\mathrm{N}/2)} = \mathrm{e}^{-j4\pi/N} = W_N^2,$$

which can be written as:

$$W_N^{k(2\mathrm{n})} = (W_N^2)^{kn} = \mathrm{W}_{N/2}^{kn} \text{ and } W_N^{k(2\mathrm{n}+1)} = W_N^k W_N^{2kn} = \mathrm{W}_{N/2}^{kn} W_N^k \qquad (3.62).$$

This gives:

$$\mathrm{X(k)} = \mathrm{G(k)} + W_N^k\, \mathrm{H(k)} \qquad \mathrm{k=0,1,...,}\ N\text{-}1 \qquad (3.63).$$

From the above equation, it can be shown that $\mathrm{X(k)}$ is formed by merging two (N /2) points DFTs G(k) and $\mathrm{X(k)}$. Equation (3.63) can be written as two groups of N /2 equations after splitting the index range $0 \le \mathrm{k} \le N$ -1 into two ranges as $N/2 \le \mathrm{K}+N/2 \le N$ -1:

$$\mathrm{X(k)} = \mathrm{G(k)} + W_N^k\, \mathrm{H(k)}$$

$$\mathrm{X(k+\,N/\,2)} = \mathrm{G(k+\,N/\,2)} + W_N^{(k+N/2)}\, \mathrm{H(k+\,N/\,2)} \qquad \mathrm{k=0,1,...,}\ N/2\text{-}1 \qquad (3.64).$$

G(k+N/2)=G(k) and H(k+N/2)=H(k) by the property of the DFT which states any size- N DFT is periodic in k with period N . Also, the twiddle factor is:

$$W_N^{N/2} = (e^{-j2\pi/N})^{N/2} = e^{-j\pi} = -1 \qquad (3.65).$$

Using the above equations, the DFT merging equations can be given as:

$$X(k) = G(k) + W_N^k H(k)$$

$$X(k+ N/ 2) = G(k) - W_N^k H(k) \qquad k=0,1,..., N/2-1 \qquad (3.66).$$

These equations are also called the butterfly merging equations [ORF]. These equations can be written in vector form as follows:

$$\begin{bmatrix} X_0 \\ X_1 \\ . \\ . \\ X_{N/2-1} \end{bmatrix} = \begin{bmatrix} G_0 \\ G_1 \\ . \\ . \\ G_{N/2-1} \end{bmatrix} + \begin{bmatrix} H_0 \\ H_1 \\ . \\ . \\ H_{N/2-1} \end{bmatrix} \times \begin{bmatrix} W_N^0 \\ W_N^1 \\ . \\ . \\ W_N^{N/2-1} \end{bmatrix} \qquad (3.67)$$

$$\begin{bmatrix} X_{N/2} \\ X_{N/2+1} \\ . \\ . \\ X_{N-1} \end{bmatrix} = \begin{bmatrix} G_0 \\ G_1 \\ . \\ . \\ G_{N/2-1} \end{bmatrix} - \begin{bmatrix} H_0 \\ H_1 \\ . \\ . \\ H_{N/2-1} \end{bmatrix} \times \begin{bmatrix} W_N^0 \\ W_N^1 \\ . \\ . \\ W_N^{N/2-1} \end{bmatrix} \qquad (3.68).$$

To summarize, the radix-2 FFT algorithm can be expressed by the following three conceptual steps [ORF]:

1) Shuffling the N -dimensional input into N one-dimensional signals;

2) Performing N one-point DFTs;

3) Merging these N one-point DFTs into a single N -point DFT.

The FFT produces a spectrum ranging from the negative Nyquist frequency (half the sampling rate) to the positive Nyquist frequency, or alternatively from the zero frequency to the sampling frequency, because of the spectrum periodicity for discrete time signals.

The zoom FFT is a technique which is used to study a portion of a spectrum at a better computational frequency resolution, for a fixed value of N . This technique is used when a better computational frequency

resolution is needed for a small portion of the whole frequency range [PRA'85], [TEC'80], [COL] (e.g., to better deal with narrowband signals such as the signals that will be processed in this thesis). The zoom FFT multiplies the sequence of samples by a complex exponential function $e^{-j2\pi f_0 t}$ to shift the frequency content around f_0 so that it appears around DC. The resulting samples go through a digital low pass filter to only keep the frequency range of interest around DC. At this stage, the signal is downsampled by a factor M, which can be called as the zoom factor. The resulting spectrum of the downsampled sequence is the spectrum region that was originally around f_0, stretched by a factor M, and now occupying the full frequency range. During the resampling process, one out of M samples is kept and the rest is discarded. The resulting samples are fed to an N-point FFT computation. This produces the zoom FFT spectrum [PRA'85].

The advantage of the zoom FFT is that using the same original N-point FFT routine it is possible to obtain a better computational frequency resolution (M time better) in a frequency region of interest. This assumes however that we are only interested to evaluate the FFT in that frequency region, which occupies 1/M of the original spectrum. If not, using the same size-N FFT, multiple zoom FFTs over different frequency regions could be used to obtain a better computational frequency resolution over a wider range of frequencies.

3.5 Mixing of different non-parametric PSD estimation methods

We introduce here a method called "MIX FFTs" which will be used for comparison with other methods in the experiments of Chapter 5. In the MIX FFTs method, the result of the power spectrum analysis from a FFT-based analysis (Welch non-parametric PSD estimation method) using a first window is combined with the result of the power spectrum analysis from a FFT-based analysis using a second window. The mixing is done in the dB magnitude domain, and the idea is to combine results providing good frequency resolution (e.g. rectangular window) with results providing low leakage (e.g. non-rectangular window). Averaging was done in the dB domain instead of the linear because in linear averaging the spectrum produced by a window with low spectral leakage property (e.g. rectangular window) will completely hide/mask the low peaks in a spectrum produced by a window with good spectral leakage characteristic (e.g. non rectangular window).

For cases where it is needed to have simultaneously the best possible frequency resolution using FFT-based methods (to distinguish closely located peaks) and the best spectral leakage characteristics for FFT-based methods (to detect weak peaks), no single window can perform satisfactorily. Thus by combining the results

from different windows in principle it becomes possible to display a power spectrum where both closely located peaks and weak peaks can be detected. The drawback of the MIX FFTs method is that the resulting display should not be used to measure the levels of the resulting components, as the averaging process in the dB domain destroys the original information about the absolute level of the different components. Thus the MIX FFTs method can only be used as a tool to indicate the presence or absence of frequency components and their frequencies, but not for amplitude or power estimation.

Chapter 4 Parametric power spectrum density estimation techniques

4.1 Concept of parametric power spectrum density estimation

Non-parametric power spectrum estimation techniques discussed in the previous chapter make use of FFT algorithm and are easy to compute. But there are some limitations which makes them inappropriate to use in certain applications [STO'05], [HAY'97]. One of the limitations is that due to finite length windowing of the data, these methods produce spectral leakage. Because of this, weak signals are masked and are difficult to detect in the estimated PSD. Other limitation is that in order to achieve a desirable frequency resolution non-parametric methods require long data records. Non-parametric power spectrum estimation techniques don't make use of the information about the data-generating process in estimating the power spectrum density [HAY'97].

Because of the above limitations, it is possible to incorporate a model of the process into the power spectrum estimation techniques to get accurate and potentially better frequency resolution. This can be achieved with the use of parametric power spectrum estimation methods [MAN'05], [ZAK'05]. As parametric methods make use of the information on the generation of the data, these methods extrapolate the values the autocorrelation for lags $m \geq N$ (as opposed to assuming that the values are zero). This can also avoid the use of window functions and in turn the spectral leakage problem. A signal generation model and its parameters can be estimated from the observed data. This model and the estimated parameters can be then used to compute the power spectrum density. These methods are mostly useful to process short data records [TCH'09], [PER'06].

Linear parametric methods makes use of a model of data $x(\mathrm{n})$ as the output of linear system represented as a system function [HAY'97]:

$$H(\mathrm{z}) = \frac{B(\mathrm{z})}{A(\mathrm{z})} = \frac{\sum_{k=0}^{q} b_k z^{-k}}{1 + \sum_{k=1}^{p} a_k z^{-k}} \tag{4.1}$$

The corresponding difference equation is:

$$x(\mathrm{n}) = -\sum_{k=1}^{p} a_k x(\mathrm{n}-\mathrm{k}) + \sum_{k=0}^{q} b_k w(\mathrm{n}-\mathrm{k})$$

where $w(\mathrm{n})$ is the input data and $\mathrm{x}(\mathrm{n})$ is the output data.

If the output data is represented as a stationary random process, then the input data is also a stationary random process. Then the power spectrum density is:

$$\Gamma_{xx}(\mathrm{f}) = |\, \mathrm{H(f)}\,|^2\ \Gamma_{ww}(\mathrm{f}) \tag{4.2}$$

where $\Gamma_{ww}(\mathrm{f})$ is the power spectrum density of the input and $\mathrm{H(f)}$ is the frequency response of the model.

Let's consider an input sequence $w(\mathrm{n})$ from a zero mean white noise process and its autocorrelation given as:

$$\gamma_{ww}(\mathrm{m}) = \sigma_w^2 \delta(\mathrm{m}) \tag{4.3}$$

where σ_w^2 is the variance.

Now, the power spectrum density can be given as:

$$\Gamma_{xx}(\mathrm{f}) = \sigma_w^2\, |\, \mathrm{H(f)}\,|^2 = \sigma_w^2 \frac{|\, B(f)\,|^2}{|\, A(f)\,|^2} \tag{4.4}.$$

The first step in determining a parametric power spectrum density is to select a suitable model for the process. This can be done with the priori information of how the data is generated or with the help of some experiments. After the model has been finalized, model parameters are estimated from the given data. The second step includes the use of these estimated parameters in parametric form to estimate the power spectrum [MAN'05], [HAY'97].

4.2 AR methods

Autoregressive moving average [ARMA(p,q)] processes of order (p,q) are generated by pole-zero models. Autoregressive [AR(p)] models of order p are generated when q=0 and $\mathrm{b}_0 = 1$ in (4.1), and the system model has an all-pole function $H(\mathrm{z}) = \dfrac{1}{A(\mathrm{z})}$. When A(z)=1, then H(z)=B(z) in (4.1) is an all-zero model and the output sequence is known as Moving average [MA(q)] model of order q [CAR'82]. This section describes AR models for PSD estimation.

AR models have some advantages over other models. They leads to a simple set of linear equations for estimation of the AR parameters [PER'93], [CAS'11], [CAR'82]. Also, they are appropriate for representing spectra with very narrow peaks [OPP'09]. Because of these advantages, AR models are used widely [SUB'07], [UBE'04]. It is important to develop the relationships between the autocorrelation function and the model parameters before explaining the AR methods [PRO'96].

For ARMA(p,q) processes, the relationship between the autocorrelation and the model parameters can be given as follows:

$$\gamma_{xx}(\mathrm{m}) = \begin{cases} -\sum_{k=1}^{p} a_k \gamma_{xx}(\mathrm{m}-\mathrm{k}), \\ -\sum_{k=1}^{p} a_k \gamma_{xx}(\mathrm{m}-\mathrm{k}) + \sigma_w^2 \sum_{k=0}^{q-m} h(\mathrm{k})\, \mathrm{b}_{k+m}, \\ \gamma_{xx}^{*}(-\mathrm{m}), \end{cases} \tag{4.4}$$

for m >q, $0 \le \mathrm{m} \le \mathrm{q}$, m <0 respectively.

For a case of m >q model parameters, the denominator coefficients a_k can be obtained by the following set of linear equations:

$$\begin{bmatrix} \gamma_{xx}(\mathrm{q}) & \gamma_{xx}(\mathrm{q}-1) & . & . & \gamma_{xx}(\mathrm{q}-\mathrm{p}+1) \\ \gamma_{xx}(\mathrm{q}+1) & \gamma_{xx}(\mathrm{q}) & . & . & \gamma_{xx}(\mathrm{q}+\mathrm{p}+2) \\ . & . & . & . & . \\ . & . & . & . & . \\ \gamma_{xx}(\mathrm{q}+\mathrm{p}-1) & \gamma_{xx}(\mathrm{q}+\mathrm{p}-2) & . & . & \gamma_{xx}(\mathrm{q}) \end{bmatrix} \begin{bmatrix} a_1 \\ a_2 \\ . \\ . \\ a_p \end{bmatrix} = \begin{bmatrix} \gamma_{xx}(\mathrm{q}+1) \\ \gamma_{xx}(\mathrm{q}+2) \\ . \\ . \\ \gamma_{xx}(\mathrm{q}+\mathrm{p}) \end{bmatrix} \tag{4.5},$$

using estimates of the autocorrelation sequence for $\gamma_{xx}(\mathrm{m})$ for $m \ge q$.

For AR(p) models, the autocorrelation and the AR parameters a_k are related as follows, by setting q=0:

$$\gamma_{xx}(\mathrm{m}) = \begin{cases} -\sum_{k=1}^{p} a_k \gamma_{xx}(\mathrm{m}-\mathrm{k}), \\ -\sum_{k=1}^{p} a_k \gamma_{xx}(\mathrm{m}-\mathrm{k}) + \sigma_w^2, \\ \gamma_{xx}^*(-\mathrm{m}), \end{cases} \tag{4.6}$$

for m>0 , m=0, and m<0, respectively.

The AR parameters a_k can be found using the Yule Walker equations:

$$\begin{bmatrix} \gamma_{xx}(0) & \gamma_{xx}(-1) & . & . & \gamma_{xx}(-\mathrm{p}+1) \\ \gamma_{xx}(1) & \gamma_{xx}(0) & . & . & \gamma_{xx}(-\mathrm{p}+2) \\ . & . & . & . & . \\ . & . & . & . & . \\ \gamma_{xx}(\mathrm{p}-1) & \gamma_{xx}(\mathrm{p}-2) & . & . & \gamma_{xx}(0) \end{bmatrix} \begin{bmatrix} a_1 \\ a_2 \\ . \\ . \\ a_k \end{bmatrix} = \begin{bmatrix} \gamma_{xx}(1) \\ \gamma_{xx}(2) \\ . \\ . \\ \gamma_{xx}(\mathrm{p}) \end{bmatrix} \tag{4.7}$$

and the variance in 4.4 is computed from:

$$\sigma_w^2 = \gamma_{xx}(0) + \sum_{k=1}^{p} a_k \gamma_{xx}(-\mathrm{k}) \tag{4.8}.$$

Equations (4.7) and (4.8) can be combined in a single matrix form as follows:

$$\begin{bmatrix} \gamma_{xx}(0) & \gamma_{xx}(-1) & . & . & \gamma_{xx}(-\mathrm{p}) \\ \gamma_{xx}(1) & \gamma_{xx}(0) & . & . & \gamma_{xx}(-\mathrm{p}+1) \\ . & . & . & . & . \\ . & . & . & . & . \\ \gamma_{xx}(\mathrm{p}) & \gamma_{xx}(\mathrm{p}-1) & . & . & \gamma_{xx}(0) \end{bmatrix} \begin{bmatrix} 1 \\ a_1 \\ . \\ . \\ a_p \end{bmatrix} = \begin{bmatrix} \sigma_w^2 \\ 0 \\ . \\ . \\ 0 \end{bmatrix} \tag{4.9}.$$

Using the Levinson-Durbin algorithm, this matrix can be inverted efficiently, as this is a Toeplitz matrix. It can thus be seen that by knowing the autocorrelation sequence $\gamma_{xx}(\mathrm{m})$ for $0 \le m \le p$, the AR(p) model parameters a_k can be easily computed. Also, the autocorrelation sequence can be extended for $m > p$ using equation (4.4) after the model parameters are determined.

4.2.1 Yule Walker Method

This method makes use of the relation and equations described above. The data autocorrelation is estimated and these estimates are used in equation (4.7) to get the AR model parameters [PRO'96]. To make sure that the autocorrelation matrix is positive semidefinite, which gives a stable AR model, a biased form of the autocorrelation estimate is used:

$$\gamma_{xx}(\mathrm{m}) = \frac{1}{N}\sum_{n=0}^{N-m-1} x^*(\mathrm{n})\,\mathrm{x}(\mathrm{n}+\mathrm{m}) \qquad m \geq 0 \qquad (4.10).$$

The power spectrum estimate is:

$$P_{xx}^{YW}(\mathrm{f}) = \frac{\sigma_{wp}^2}{|1+\sum_{k=1}^{p}\hat{a}(\mathrm{k})\,\mathrm{e}^{-j2\pi fk}\,|^2} \qquad (4.11)$$

where the AR parameters $\hat{a}(\mathrm{k})$ estimates are computed by using the Levinson-Durbin algorithm. Lacoss (1971) proved that in an AR spectrum estimate the spectral peaks are proportional to the square of the power of the sinusoidal signal, whereas the area under the peak is proportional to the power of the sinusoid [PRO'96].

4.2.2 Burg Method (Maximum Entropy method)

In the Burg algorithm, the all-pole model parameters are determined by minimizing the sum of squares of the forward and backward prediction errors, with the constraint that AR parameters satisfy the Levinson-Durbin algorithm. This minimization is performed sequentially with respect to the reflection coefficients to stabilize the model [HAY'97], [PRO'96].

For a given data $x(\mathrm{n})$, n=0,1,..., N -1, the forward and backward linear prediction estimates of order m are:

$$\bar{x}(\mathrm{n}) = -\sum_{k=1}^{m} a_m(\mathrm{k})\,\mathrm{x}(\mathrm{n}-\mathrm{k}) \qquad (4.12)$$

$$\bar{x}(\mathrm{n}-\mathrm{m}) = -\sum_{k=1}^{m} a_m^*(\mathrm{k})\,\mathrm{x}(\mathrm{n}+\mathrm{k}) \tag{4.13}$$

Now the forward and backward linear prediction errors are respectively:

$$f_m(\mathrm{n}) = \mathrm{x}(\mathrm{n}) - \bar{x}(\mathrm{n}) \tag{4.14}$$

$$g_m(\mathrm{n}) = \mathrm{x}(\mathrm{n}-\mathrm{m}) - \bar{x}(\mathrm{n}-\mathrm{m}) \tag{4.15}$$

where $a_m(k)$ are the prediction coefficients for $0 \le k \le m-1$, m=1,2,...,p.

The least squares error is:

$$\mathrm{E}_m = \sum_{n=m}^{N-1} [\,|\, g_m(\mathrm{n}) \,|^2 + |\, \mathrm{f}_m(\mathrm{n}) \,|^2\,] \tag{4.16}$$

The least squares error is minimized by the prediction coefficients satisfying the Levinson Durbin recursion:

$$a_m(k) = a_{m-1}(k) + K_m a_{m-1}^*(\mathrm{m}-k) \qquad 1 \le k \le m-1$$

$$1 \le m \le p \tag{4.17}$$

where K_m is the m^{th} reflection coefficient in a lattice filter realization of the predictor and $K_m = a_m(\mathrm{m})$. With respect to complex valued reflection coefficient K_m, a minimization of E_m can be done, leading to:

$$\overline{K}_m = \frac{\sum_{n=m}^{N-1} f_{m-1}(\mathrm{n})\, \mathrm{g}_{m-1}^*(\mathrm{n}-1)}{\frac{1}{2}\sum_{n=m}^{N-1} [\,|\, g_{m-1}(\mathrm{n}) \,|^2 + |\, \mathrm{f}_{m-1}(\mathrm{n}-1) \,|^2\,]} \qquad \mathrm{m}=1,2,\ldots,\mathrm{p} \tag{4.18}$$

The numerator in equation (4.18) is the crosscorrelation of the forward and backward errors. The all-pole model is always stable, as $|K_m|<1$ due to normalization factors in the denominator. It can be seen that the denominator is the least squares estimate of the forward and backward errors. Therefore, equation (4.18) can be written as:

$$\overline{K}_m = \frac{\sum_{n=m}^{N-1} f_{m-1}(\mathrm{n})\, \mathrm{g}^*_{m-1}(\mathrm{n}-1)}{\frac{1}{2}\left[\overline{E}^f_{m-1} + \overline{E}^b_{m-1}\right]} \qquad \mathrm{m}=1,2,...,\mathrm{p} \qquad (4.19)$$

where $\overline{E}^f_{m-1}$ and $\overline{E}^b_{m-1}$ are least squares forward and backward error estimates.

Using equation (4.19), i.e., reflection coefficients and AR model parameter estimates from the Levinson-Durbin algorithm, the Burg power spectrum density estimate is then [PRO'96]:

$$\mathrm{P}^{BU}_{xx}(\mathrm{f}) = \frac{\overline{E}_p}{|1 + \sum_{k=1}^{p} \widehat{a_p}(\mathrm{k})\, \mathrm{e}^{-j2\pi fk}\ |^2} \qquad (4.20).$$

The Burg power spectrum estimation is also known as the Maximum Entropy spectrum estimation [CHA'90]. To make the autocorrelation sequence positive semidefinite for values $m > p$ from the given autocorrelation sequence $0 \le m \le p$, an extrapolation is done using the maximum entropy, such that the spectrum of the process is flat for all spectra of the given autocorrelation values $\gamma_{xx}(\mathrm{m})$, $0 \le m \le p$. When the exact autocorrelation values are known, the Burg power spectrum density is identical to the AR model spectrum [PRO'96].

The Burg method provides a good frequency resolution and a stable AR model. Also, its computational complexity is small. However, it often produces spurious peaks for higher order models. For short data records, this method is sensitive to the initial phase of sinusoids found in signals. This in effect shifts the frequency of a sinusoid from its true location in the estimated PSD. The Burg method can also produce a line splitting effect at high signal to noise ratios for sinusoids in noise scenarios, i.e., the spectrum of the signal shows multiple closely spaced peaks for what should be a single peak in the spectra [PRO'96]. These drawbacks can be made less severe with some modifications. For example, windowing or weighing can be done on the squared forward and backward errors, i.e., least square optimization of weighted squared errors.

4.2.3 Minimum Covariance Method

The minimum covariance method is another technique for estimating the AR parameters. A set of linear equations is used in this method:

$$\begin{bmatrix} \gamma_{xx}(1,1) & \gamma_{xx}(2,1) & . & . & \gamma_{xx}(\mathrm{p},1) \\ \gamma_{xx}(1,2) & \gamma_{xx}(2,2) & . & . & \gamma_{xx}(\mathrm{p},2) \\ . & . & . & . & . \\ . & . & . & . & . \\ \gamma_{xx}(1,\mathrm{p}) & \gamma_{xx}(2,\mathrm{p}) & . & . & \gamma_{xx}(\mathrm{p},\mathrm{p}) \end{bmatrix} \begin{bmatrix} a_p(1) \\ a_p(2) \\ . \\ . \\ a_p(\mathrm{p}) \end{bmatrix} = \begin{bmatrix} \gamma_{xx}(0,1) \\ \gamma_{xx}(0,2) \\ . \\ . \\ \gamma_{xx}(0,\mathrm{p}) \end{bmatrix} \tag{4.21}$$

where

$$\gamma_{xx}(\mathrm{l},\mathrm{m}) = \sum_{n=p}^{N-1} x^*(\mathrm{n}-\mathrm{l})\,\mathrm{x}(\mathrm{n}-\mathrm{m}).$$

For short data sequences, the covariance method can produce a better frequency resolution in the spectrum estimates than the Yule Walker method, as it doesn't require windowing of the data for estimating the autocorrelation sequence estimates. But for longer data records the effect of windowing on the data becomes negligible. Also, the matrix formed in the above equation is not Toeplitz, unlike the Yule Walker method, therefore the covariance method requires more computations.

The modified covariance method is similar to the covariance method except that the modified covariance method minimizes the sum of squares of the forward and backward prediction errors, instead of only minimizing the sum of squares of the forward prediction error. Like the covariance method it does not require windowing the data. The AR parameters in this method are found by equation (4.21) and a set of linear equations as given below:

$$\gamma_{xx}(\mathrm{l},\mathrm{m}) = \sum_{n=p}^{N-1} [x^*(\mathrm{n}-m)\,\mathrm{x}(\mathrm{n}-l) + x^*(\mathrm{n}-p+l)\,\mathrm{x}(\mathrm{n}-p+m)] \tag{4.22}.$$

In principle, the covariance method and modified covariance method can show less line splitting and spurious peaks in their estimated PSDs, and the peak locations are less sensitive to the initial phase of the sinusoids [PRO'96].

4.3 Overview of MA model

From the discussion in section 4.2, equation (4.6) gives the pole parameters a_k but not the MA parameters b_k. The equation below depends on the impulse response h(n) which can be represented in terms of parameters b_k by performing a long division of B(z) with a known A(z). This leads to a set of nonlinear equations for determining the MA parameters [STO'05], [HAY'97], [PRO'96].

$$\sigma_w^2 \sum_{k=0}^{q-m} h(\mathrm{k})\, \mathrm{b}_{k+m} = \gamma_{xx}(\mathrm{m}) + \sum_{k=1}^{p} \gamma_{xx}(\mathrm{m}-\mathrm{k}) a_k \qquad 0 \le m \le q \tag{4.23}$$

The autocorrelation sequence is related to the MA parameters b_k as follows:

$$\gamma_{xx}(\mathrm{m}) = \begin{cases} \sigma_w^2 \sum_{k=0}^{q} b_k b_{k+m}, \\ 0, \\ \gamma_{xx}^*(-\mathrm{m}), \end{cases} \tag{4.24}$$

for $0 \le m \le q$, m>q, m<0 respectively.

However, defining

$$\mathrm{B(z)\,B(z^{-1}) = D(z) = \sum_{m=-q}^{q} d_m z^{-m}}$$

the MA parameters are related to the coefficients d_m by the equation:

$$d_m = \sum_{k=0}^{q-|m|} b_k b_{k+m}, \qquad |\, m \,| \le q \tag{4.25}.$$

Then,

$$\gamma_{xx}(\mathrm{m}) = \begin{cases} \sigma_w^2 d_m, \\ 0, \end{cases}$$

for $|m| \leq q$ and $|m| > q$ respectively.

From the above equations, the MA(q) process power spectrum is:

$$\Gamma_{xx}^{MA}(\mathrm{f}) = \sum_{m=-q}^{q} \gamma_{xx}(\mathrm{m})\, \mathrm{e}^{-j2\pi fm} \tag{4.26}$$

It can be seen that for $|m| \leq q$ the autocorrelation estimates $\gamma_{xx}(\mathrm{m})$ are sufficient for estimating the MA power spectrum density, which is then similar to non-parametric methods:

$$P_{xx}^{MA}(\mathrm{f}) = \sum_{m=-q}^{q} \gamma_{xx}(\mathrm{m})\, \mathrm{e}^{-j2\pi fm} \tag{4.27}$$

4.4 Overview of ARMA model

ARMA models are often suitable for signals corrupted with noise [PRO'96], [BRO'06], [CHO'02]. As discussed in section 4.2, equation (4.4) shows the relationship between ARMA model parameters and the autocorrelation function. The AR parameters a_k can be found for lags |m|>q and by substituting estimates of the autocorrelation function. Because of the poor estimates of the autocorrelation function for large lags, this method provides inaccurate estimates of AR parameters for large lags.

So to avoid this, for autocorrelation sequence for lags M where M>p+q, the following can be used:

$$\begin{bmatrix} \gamma_{xx}(\mathrm{q}) & \gamma_{xx}(\mathrm{q-1}) & . & . & \gamma_{xx}(\mathrm{q-p+1}) \\ \gamma_{xx}(\mathrm{q+1}) & \gamma_{xx}(\mathrm{q}) & . & . & \gamma_{xx}(\mathrm{q-p+2}) \\ . & . & . & . & . \\ . & . & . & . & . \\ \gamma_{xx}(\mathrm{M-1}) & \gamma_{xx}(\mathrm{M-2}) & . & . & \gamma_{xx}(\mathrm{M-p}) \end{bmatrix} \begin{bmatrix} a_1 \\ a_2 \\ . \\ . \\ a_p \end{bmatrix} = \begin{bmatrix} \gamma_{xx}(\mathrm{q+1}) \\ \gamma_{xx}(\mathrm{q+2}) \\ . \\ . \\ \gamma_{xx}(\mathrm{M}) \end{bmatrix} \tag{4.28}$$

which is,

$$R_{xx}a = -\gamma_{xx} \tag{4.29},$$

where R_{xx} has a dimension (M-q) x p and M-q>p. The parameter vector $\bar{a}$ can be determined using least squares minimization:

$$\bar{a} = -(R^T{}_{xx}R_{xx})^{-1}R^T{}_{xx}\gamma_{xx} \tag{4.30}$$

This is known as the least squares modified Yule Walker method. After estimating the AR model parameters, we get following system,

$$\bar{A}(\mathrm{z}) = 1 + \sum_{k=1}^{p}\bar{a}_k z^{-k} \tag{4.31}.$$

Using the above filter, the data sequence can be filtered:

$$v(\mathrm{n}) = x(\mathrm{n}) + \sum_{k=1}^{p}\bar{a}_k x(\mathrm{n}-\mathrm{k}) \qquad \mathrm{n}=0,1,\ldots,\ N-1 \tag{4.32}.$$

The MA spectrum is then obtained from the filtered data v(n) for $p \le n \le N-1$, from an estimate of the autocorrelation sequence $\gamma_{vv}(\mathrm{m})$ (similar to non-parametric estimation):

$$\mathrm{P}_{vv}^{MA}(\mathrm{f}) = \sum_{m=-q}^{q}\gamma_{vv}(\mathrm{m})e^{-j2\pi fm} \tag{4.33}.$$

The important things to notice in the above equation are that the power spectrum can be determined without computing the parameters b_k, and that $\gamma_{vv}(\mathrm{m})$ is an estimate of the autocorrelation function for the MA model. Using these relations the ARMA power spectrum density is given as follows [PRO'96]:

$$\bar{\mathrm{P}}_{xx}^{ARMA}(\mathrm{f}) = \frac{P_{vv}^{MA}(\mathrm{f})}{|1 + \sum_{k=1}^{p}\bar{a}_k e^{-j\pi 2fk}|^2} \tag{4.34}.$$

4.5 Overview of Harmonic methods

Harmonic methods deal with sinusoid signals corrupted by additive white noise [PRO'96]. These methods use eigen-decomposition of a correlation matrix of the noisy signal [CAS'11]. A difference equation of a signal made up of p sinusoidal components is given as [PRO'96]:

$$x(\mathrm{n}) = -\sum_{m=1}^{2p} a_k x(\mathrm{n}-m) \tag{4.35}$$

and its system function is:

$$H(\mathrm{z}) = \frac{1}{1+\sum_{m=1}^{2p} a_m z^{-m}} \tag{4.36}$$

where A(z)=$1+\sum_{m=1}^{2p} a_m z^{-m}$.

This polynomial has 2p roots on the unit circle corresponding to the sinusoid frequencies. Now,

$$y(\mathrm{n}) = x(\mathrm{n}) + \mathrm{w}(\mathrm{n}) \tag{4.37}$$

where w(n) is white noise with $E[|\,\mathrm{w}(\mathrm{n})\,|^2] = \sigma_w^2$.

Using equation (4.37) to get $x(\mathrm{n})$ and substituting it in equation (4.35) we get:

y(n)-w(n)=$-\sum_{m=1}^{2p} a_m[\mathrm{y}(\mathrm{n}-\mathrm{m}) - \mathrm{w}(\mathrm{n}-\mathrm{m})]$

i.e.,

$$\sum_{m=0}^{2p} a_m\, \mathrm{y}(\mathrm{n}-\mathrm{m}) = \sum_{m=0}^{2p} a_m\, \mathrm{w}(\mathrm{n}-\mathrm{m}) \tag{4.38}.$$

Equation (4.38) is a difference equation for an ARMA(p,p) process with identical AR and MA parameters. Equation (4.38) in matrix form is:

$$Y^T a = W^T a \tag{4.39}$$

where Y^T =[y(n) y(n-1) ... y(n-2p)], W^T =[w(n) w(n-1) ...w(n-2p)], a =[1 a_1 a_2 ... a_{2p}] are the observed data vector, the noise vector and the coefficient vector, respectively.

Multiplying equation (4.39) by Y and taking its expected value while considering $\mathrm{w(n)}$ as zero mean white noise and X as a deterministic signal:

$$E(YY^T)a = E(YW^T)a = E[(\mathrm{X+W})\,\mathrm{W}^T]a$$

$$\Gamma_{yy} a = \sigma_w^2 a \tag{4.40}.$$

Equation (4.40) is in the eigen-equation form:

$$(\Gamma_{yy} - \sigma_w^2 I)a = 0 \tag{4.41}$$

where σ_w^2 is an eigenvalue of the autocorrelation matrix Γ_{yy} and vector a is an eigenvector corresponding to eigenvalue σ_w^2.

4.5.1 Pisarenko Harmonic Decomposition Method

The Pisarenko harmonic decomposition method makes use of the noise subspace eigenvector to estimate the sinusoids frequencies [PRO'96].

Equation (4.41) in the previous section is the basis of the Pisarenko harmonic decomposition method. The autocorrelation values for *p* randomly phased sinusoids in additive white noise are,

$$\gamma_{yy}(0) = \sigma_w^2 + \sum_{i=1}^{p} P_i \tag{4.42}$$

$$\gamma_{yy}(\mathrm{k}) = \sum_{i=1}^{p} P_i \cos 2\pi f_i k \qquad k \neq 0 \tag{4.43}$$

where $P_i = A_i^2/2$ and A_i are the average power for the i^{th} sinusoid and its corresponding amplitude, respectively. Equation (4.43) can also be written as:

$$\begin{bmatrix} \cos 2\pi f_1 & \cos 2\pi f_2 & . & . & \cos 2\pi f_p \\ \cos 4\pi f_1 & \cos 4\pi f_2 & . & . & \cos 2\pi f_p \\ . & . & . & . & . \\ . & . & . & . & . \\ \cos 2\pi pf_1 & \cos 2\pi f_2 & . & . & \cos 2\pi pf_p \end{bmatrix} \begin{bmatrix} P_1 \\ P_2 \\ . \\ . \\ P_p \end{bmatrix} = \begin{bmatrix} \gamma_{yy}(1) \\ \gamma_{yy}(2) \\ . \\ . \\ \gamma_{yy}(\mathrm{p}) \end{bmatrix} \tag{4.44}$$

This equation can be used to calculate sinusoids power, if frequencies $1 \le i \le p$ are known and estimates of the autocorrelation can be used. The variance of the noise can be determined by equation (4.45):

$$\sigma_w^2 = \gamma_{yy}(0) - \sum_{i=1}^{p} P_i \tag{4.45}$$

The variance σ_w^2 corresponds to minimum eigenvalue of Γ_{yy} for ARMA processes of p sinusoids in white noise, when the autocorrelation matrix dimension is equal or greater than (2p+1) x (2p+1). Then the minimum eigenvalues gives the eigenvectors which in turn provide the ARMA coefficient vectors. Hence, frequencies can be obtained from polynomial roots using the equation:

$$\mathrm{A(z)} = 1 + \sum_{m=1}^{2p} a_m z^{-m}$$

for $1 \le i \le p$, where the minimum eigenvalues σ_w^2 produce coefficients corresponding their respective eigenvector. This method was developed by Pisarenko (1989).

The Pisarenko method can be summarized as follows [PRO'96]:

1) From the given data, estimate Γ_{yy}.

2) Find the minimum eigenvalues and the corresponding minimum eigenvectors, which in turn gives the ARMA(2p,2p) model parameters.

3) Calculate the roots corresponding to the frequencies.

4) By solving equation (4.44), provide signal powers by substituting the autocorrelation estimates.

4.5.2 MUSIC Algorithm

Before introducing the MUSIC algorithm, it is necessary to discuss eigen-decomposition of autocorrelation matrices for sinusoids in white noise [PRO'96], [HAY'97]. Consider a signal made of p complex sinusoids:

$$x(\mathrm{n}) = \sum_{i=1}^{p} A_i e^{j(2\pi \mathrm{f}_i \mathrm{n} + \phi_i)}$$

where A_i and f_i are unknown amplitudes and frequencies respectively. The phases ϕ_i are statistically independent random variables distributed evenly on $(0,2\pi)$. The autocorrelation of $x(\mathrm{n})$ which is wide sense stationary is:

$$\gamma_{xx}(\mathrm{m}) = \sum_{i=1}^{p} P_i e^{j2\pi \mathrm{f}_i m} \tag{4.46}$$

where P_i is the power of i^{th} sinusoid and $P_i = A_i^2$.

For an observed sequence $y(\mathrm{n}) = x(\mathrm{n}) + \mathrm{w}(\mathrm{n})$, where $\mathrm{w}(\mathrm{n})$ is white noise with power spectral density σ_w^2, the autocorrelation is:

$$\gamma_{yy}(\mathrm{m}) = \gamma_{xx}(\mathrm{m}) + \sigma_w^2 \delta(\mathrm{m}) \qquad \mathrm{m}=0,\pm1,\ldots,\pm(\mathrm{M}-1) \tag{4.47}$$

and therefore the autocorrelation matrix is:

$$\Gamma_{yy} = \Gamma_{xx} + \sigma_w^2 I \tag{4.48}.$$

This matrix has dimensions of M x M, Γ_{xx} is the signal $x(\mathrm{n})$ autocorrelation matrix, and $\sigma_w^2 I$ is the noise autocorrelation matrix. Γ_{xx} can be expressed as:

$$\Gamma_{xx} = \sum_{i=1}^{p} P_i s_i s_i^H \tag{4.49}$$

where s_i is a signal vector of dimension M:

$s_i = [1, e^{j2\pi f_i}, ..., e^{j2\pi(M-1)f_i}]$.

The matrix Γ_{xx} has rank p, as each $s_i s_i^H$ has a rank 1 and there are p such vector products. For real sinusoids, Γ_{xx} has rank $2p$.

For eigen-decomposition of the Hermitian matrix Γ_{yy}, suppose that the eigenvalues λ_i are arranged in decreasing order $\lambda_1 \geq \lambda_2 \geq ... \geq \lambda_m$ and $[v_i, i = 1.....M]$ are the corresponding eigenvectors, where $[v_i^H . v_j = \delta_{ij}]$. The eigenvalues λ_i for i=1,2,...,p are nonzero, whereas $\lambda_{p+1} = \lambda_{p+2} = ... = \lambda_M = 0$ (in theory, when there is no noise). From these conditions, the correlation matrix of the signal can be given as:

$$\Gamma_{xx} = \sum_{i=1}^{p} \lambda_i v_i v_i^H \tag{4.50}$$

The eigenvectors $[v_i, i = 1,..., p]$ and the signal vectors s_i, i=1,2,...,p span the signal subspace. These p eigenvectors and the corresponding eigenvalues are called the principal eigenvectors and the principal eigenvalues, respectively. Equation (4.48) can be written as follows when considering noise:

$$\sigma_w^2 I = \sigma_w^2 \sum_{i=1}^{p} v_i v_i^H \tag{4.51}$$

From equation (4.50) and (4.51), we can rewrite equation (4.48) as:

$$\Gamma_{yy} = \sum_{i=1}^{p} \lambda_i v_i v_i^H + \sum_{i=1}^{p} \sigma_w^2 v_i v_i^H$$

$$= \sum_{i=1}^{p} (\lambda_i + \sigma_w^2) v_i v_i^H + \sum_{i=p+1}^{M} \sigma_w^2 v_i v_i^H \tag{4.52}$$

The signal subspace is spanned by the principal eigenvectors $[v_i, i = 1.....p]$ and $[v_i, i = p+1....., M]$ are the eigenvectors belonging to the noise subspace, which are orthogonal to the principal eigenvectors. This is possible because of the eigen-decomposition done above and the Hermitian nature of the correlation matrix.

This discussion can be extended to explain the multiple signal classification (MUSIC) algorithm, which is a noise subspace frequency estimator [HAY'97], [PRO'96]. Consider the weighted spectral estimate:

$$P(\mathrm{f}) = \sum_{k=p+1}^{M} w_k \mid s^H(\mathrm{f}) v_k \mid^2 \tag{4.52}$$

where $[\mathrm{v}_k, \mathrm{k} = p+1 ....., \mathrm{M}]$, s(f) and w_k are the eigenvectors in the noise subspace, a complex sinusoidal vector and positive weights, respectively, with $s(\mathrm{f}) = [1, .\mathrm{e}^{2\pi jf}, ..., e^{2\pi j(\mathrm{M}-1)\mathrm{f}}]$.

For f=$\mathrm{f_i}$, $s(\mathrm{f}_i) = \mathrm{s}_i$ which is orthogonal to v_k, and this means that for the p sinusoidal frequencies we have:

$P(\mathrm{f}_i) = 0$ i=1,2,..., p.

Taking the reciprocal of P(f) gives a function with sharp peaks in frequency:

$$\frac{1}{P(\mathrm{f})} = \frac{1}{\sum_{k=p+1}^{M} w_k \mid s^H(\mathrm{f})\, \mathrm{v}_k \mid^2} \tag{4.53}.$$

If for all k weights $\mathrm{w_k}$ =1, the MUSIC PSD estimation method is obtained, which is a modified version of equation (4.53):

$$\mathrm{P}_{MUSIC}(\mathrm{f}) = \frac{1}{\sum_{k=p+1}^{M} \mid s^H(\mathrm{f})\, \mathrm{v}_k \mid^2} \tag{4.54}.$$

This method was developed by Schmidt (1981, 1986). Peaks of $\mathrm{P}_{MUSIC}(\mathrm{f})$ are the sinusoidal frequencies estimates. The power of each sinusoid can be calculated after the frequencies are obtained by the help of equation (4.44).

4.5.3 ESPRIT Algorithm

The Estimation of Signal Parameters via Rotational Invariance Techniques (ESPRIT) is also a method based on eigen-decomposition to estimate sinusoid frequencies. It makes use of the rotational invariance of signal subspaces spanned by two displaced data vectors [PRO'96].

Consider the same p complex valued sinusoids in additive white noise as in the MUSIC algorithm. By defining a time displaced vector z(n)=y(n+1), deterministic characteristics of sinusoids can be determined:

$$z(\mathrm{n}) = [\mathrm{z(n)}, \mathrm{z(n+1)}.....\mathrm{z(n+M-1)}]^T$$

$$= [\mathrm{y(n+1)}, \mathrm{y(n+2)}.....\mathrm{y(n+M)}]^T .$$

Now we can define the vectors y(n) and z(n) as follows:

$$\mathrm{y(n)} = Sa + w(\mathrm{n}) \tag{4.55}$$

$$\mathrm{z(n)} = S\phi a + w(\mathrm{n}) \tag{4.56}$$

where,

$a = [a_1,.....a_p]^T$, $a_i = A_i e^{ji\phi}$ and ϕ is defined as follows, which is a relative phase between successive time samples of each complex sinusoid and a diagonal p x p matrix:

$$\phi = diag[\mathrm{e}^{j2\pi f_1}, \mathrm{e}^{j2\pi f_2} .....\mathrm{e}^{j2\pi f_p}] .$$

ϕ is a rotational operation of vectors y(n) and z(n) which is unitary. Matrix S is the Vandermonde matrix of the column vector of dimension M x p, with:

$$s_i = [1, \mathrm{e}^{j2\pi f_1}, \mathrm{e}^{j4\pi f_i} .....\mathrm{e}^{j2\pi(\mathrm{M}-1) f_i}] \qquad \mathrm{i=1,2,..., p.}$$

The autocovariance matrix of the data vector y(n) is:

$$\Gamma_{yy} = E[\mathrm{y(n)\, y}^H(\mathrm{n})]$$

$$= \mathrm{SPS}^H + \sigma_w^2 I \tag{4.57}$$

where the matrix P is the power of the complex sinusoids, with p x p dimension and diagonal:

$$\mathrm{P} = diag[|\, a_1 \,|^2, |\, a_2 \,|^2, ... |\, a_p \,|^2]$$

$$= \mathrm{diag}[\mathrm{P}_1, \mathrm{P}_2 .....\mathrm{P}_p] .$$

The ESPRIT algorithm can be applied to the cases a covariance matrix is calculated from finite data measurements, because the method can work without the P matrix being diagonal. The crosscovariance matrix of the signal vectors y(n) and z(n) is as follows:

$$\Gamma_{yz} = E[\mathrm{y(n)}\,\mathrm{z}^{H}(\mathrm{n})] = \mathrm{SPS}^{H}\,\phi^{H} + \Gamma_{w} \tag{4.58}$$

$$\text{and } \Gamma_{w} = E[\mathrm{w(n)}\,\mathrm{w}^{H}(\mathrm{n+1})] = \sigma_{w}^{2}\begin{bmatrix} 0 & 0 & 0 & .. & 0 \\ 1 & 0 & 0 & .. & 0 \\ 0 & 1 & 0 & .. & 0 \\ . & . & . & .. & . \\ 0 & 0 & 0 & .. & 0 \end{bmatrix} \equiv \sigma_{w}^{2} Q \tag{4.59}.$$

The elements of the crosscovariance and autocovariance matrices are as follows:

$$\Gamma_{yy} = \begin{bmatrix} \gamma_{yy}(0) & \gamma_{yy}(1) & . & .. & \gamma_{yy}(\mathrm{M-1}) \\ \gamma_{yy}^{*}(1) & \gamma_{yy}(0) & . & .. & \gamma_{yy}(\mathrm{M-2}) \\ . & . & . & .. & . \\ . & . & . & .. & . \\ \gamma_{yy}^{*}(\mathrm{M-1}) & \gamma_{yy}(\mathrm{M-2}) & . & .. & \gamma_{yy}(0) \end{bmatrix} \tag{4.60}$$

$$\Gamma_{yz} = \begin{bmatrix} \gamma_{yy}(1) & \gamma_{yy}(2) & . & .. & \gamma_{yy}(\mathrm{M}) \\ \gamma_{yy}(0) & \gamma_{yy}(1) & . & .. & \gamma_{yy}(\mathrm{M-1}) \\ . & . & . & .. & . \\ . & . & . & .. & . \\ \gamma_{yy}^{*}(\mathrm{M-2}) & \gamma_{yy}^{*}(\mathrm{M-3}) & . & .. & \gamma_{yy}(1) \end{bmatrix} \tag{4.61}.$$

Both of the above matrices are Toeplitz, and $\gamma_{yy}(\mathrm{m}) = \mathrm{E}[\mathrm{y}^{*}(\mathrm{n})\,\mathrm{y(n+m)}]$.

The matrix SPS^{H} has rank p and Γ_{yy} has (M-p) eigenvalues equal to σ_{w}^{2}. Therefore,

$$\Gamma_{yy} - \sigma_{w}^{2} I = \mathrm{SPS}^{H} \equiv C_{yy} \tag{4.62}$$

and,

$$\Gamma_{yz} - \sigma_{w}^{2}\Gamma_{w} = \mathrm{SPS}^{H}\,\phi^{H} \equiv C_{yz} \tag{4.63}.$$

The above two equations can be written as follows:

$$C_{yy} - \lambda C_{yz} \equiv SP(\mathrm{I} - \lambda \phi^H)\mathrm{S}^H \tag{4.64}$$

$C_{yy} - \lambda C_{yz}$ has rank p. The eigenvalues of the matrices C_{yy}, C_{yz} are $\lambda_i = \exp(2\pi \mathrm{j} f_i)$ for i=1,2,...,p. Hence, these p eigenvalues are elements of the rotation operator ϕ lying on the unit circle. The matrices C_{yy}, C_{yz} have M-p remaining eigenvalues corresponding to the null space.

From the above discussion, the ESPRIT algorithm to determine frequencies $\{f_i\}$ can be summarized as follows [PRO'96]:

1) Calculate autocorrelation values $\gamma_{yy}(\mathrm{m})$, m=1,2,...,M to form matrices R_{yy} and R_{yz} from Γ_{yy} and Γ_{yz} estimates.

2) Calculate eigenvalues of R_{yy}. For M>p, the minimum eigenvalues are an estimate of σ_w^2.

3) Compute $\overline{C}_{yy} = R_{yy} - \overline{\sigma}_w^2 I$ and $\overline{C}_{yz} = R_{yz} - \overline{\sigma}_w^2 Q$.

4) Calculate generalized eigenvalues of the matrices $\overline{C}_{yy}, \overline{C}_{yz}$. The sinusoidal frequencies are obtained by the estimated parameters of ϕdetermined by the p generalized eigenvalues of the above matrices lying on the unit circle and the remaining M-p eigenvalues will be near the origin.

4.6 Mixing of non-parametric and parametric PSD estimation methods

Similarly to section 3.5 where a method called "MIX FFTs" was introduced combining the non-parametric PSD estimation results obtained from different windows, here we also introduce a method called "MIX FFT and MUSIC", which combines the results obtained from an FFT-based analysis (e.g. Welch non-parametric PSD estimation method) with the results from a parametric PSD estimation method (e.g. MUSIC algorithm). The mixing is done in the dB magnitude domain. The results of the FFT-based methods are normally more robust and reliable (as will be seen in Chapter 5), while the results of the MUSIC method often show peaks that are sharper and more narrow. Thus for visual displays it may sometimes be useful to combine the two results. The averaging of the two methods is performed in the dB magnitude domain, with a 50% weight applied for each method.

As in the MIX FFTs method, the drawback of the MIX FFT and MUSIC method is that the resulting display should not be used to measure the levels of the resulting components, as the averaging process in the dB domain destroys the original information about the absolute level of the different components. Thus the MIX FFT and MUSIC method can only be used as a tool to indicate the presence or absence of frequency components and their frequencies, but not for amplitude or power estimation.

Chapter 5 Simulation Results with Power Spectrum Density Estimates

5.1 Comparison of results for different parametric PSD estimation methods

Parametric methods are mostly useful to detect a fairly small number of peaks (<50, more often < 20 or even less). The range of wavelengths that can be covered by a wavemeter is fairly wide, for example from 1270 nm to 1680 nm. Within that range thousands of discrete laser frequencies could be fitted. Therefore, to consider a range of frequencies where a limited number of closely located laser frequencies are found, we considered the range 1530nm-1530.5nm. This required to perform some fairly extreme downsampling from the original 632.9907 nm sampling wavelength. For example, a downsampling factor of 6000 and an anti-aliasing filter of size 350,000 were required to produce the results of this section. With such extreme processing, the length of the filter response becomes even longer than the length of the original data from the interferometer: 300,000 samples, corresponding to a total mirror displacement of 0.18989721m at 632.9907 nm sampling wavelength. So small effects such as keeping or discarding the transients at the beginning and end of the filtered signal become critical. In the most extreme cases such as the one considered here, the filtered signal only consists of transients (no true steady state), on which the power spectrum analysis then needs to be made.

Four AR methods were first compared: the Burg method, the covariance method, the Modified Covariance method and the Yule-Walker method. In all cases there are 11 laser wavelengths positioned between 1530nm-1530.5nm (synthetically Matlab-generated sinusoidal signals with same amplitude and random phase) and we set the AR model order to 11.

Although theoretically each of the four AR methods have advantages and disadvantages, as mentioned in Chapter 4, for the setup that we use here it is clear from Figures 5.1 to 5.4 that they all produce exactly the same performance. Therefore, the simplest method to implement was selected for future testing and for C code implementation: the Yule-Walker method. Although we don't observe any "line splitting" problem in Figures 5.1 to 5.4 because the correct model order 11 was used (instead of a model order higher than the actual number of laser frequencies found in the signal), the results in the figures are not too satisfying, because the distance between the peaks amplitudes and the valleys is so small that it would prevent the use of the AR PSD estimates in practice, since a good gap between the peaks and the valleys is required to allow for different signal levels. This means that the use of AR methods would need to be restricted to

either more narrow frequency ranges, or for cases where the number of peaks to detect is lower than the 11 peaks considered here. We will consider such cases later in this chapter.

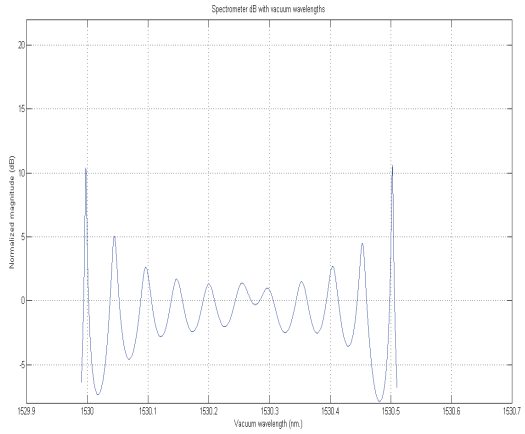

Figure 5.1:PSD by Burg method for 11 wavelengths and order of 11

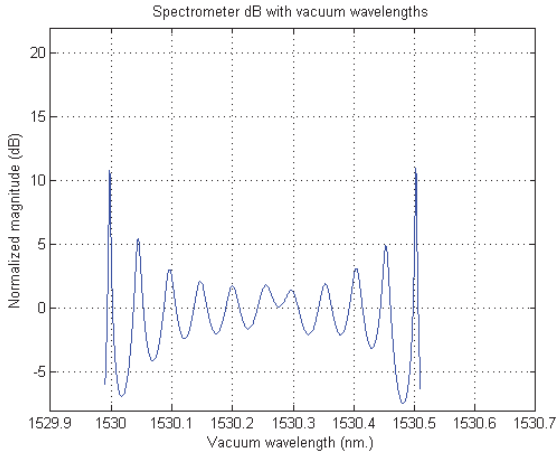

Figure 5. 2:PSD by Covariance method for 11 wavelengths and order of 11

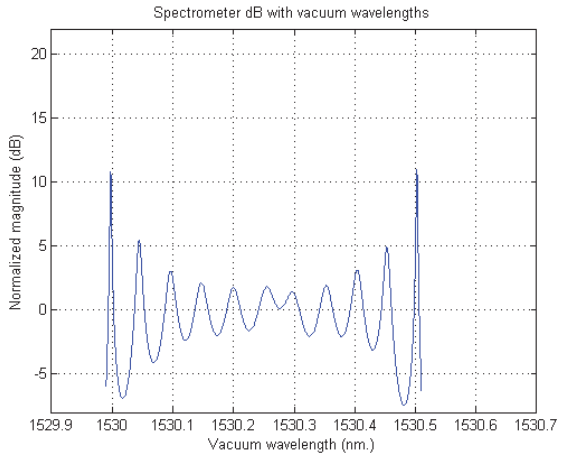

Figure 5. 3:PSD by Modified Covariance method for 11 wavelengths and order of 11

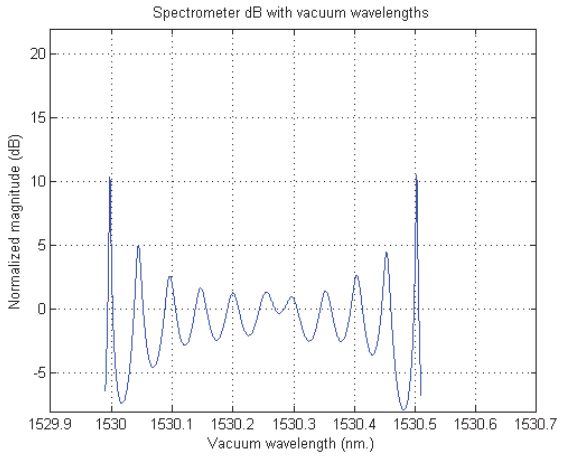

Figure 5. 4:PSD by Yule-Walker Method for 11 wavelengths and order of 11

The ARMA and MA PSD estimates were not implemented because of the tonal/peaky spectral nature of the sinusoid signals that were are trying to detect for the wavemeter application. For the harmonic PSD estimation methods, we considered the MUSIC algorithm, because it lead to a simple implementation in the C code. Figure 5.5 below shows the result for the MUSIC method PSD estimate.

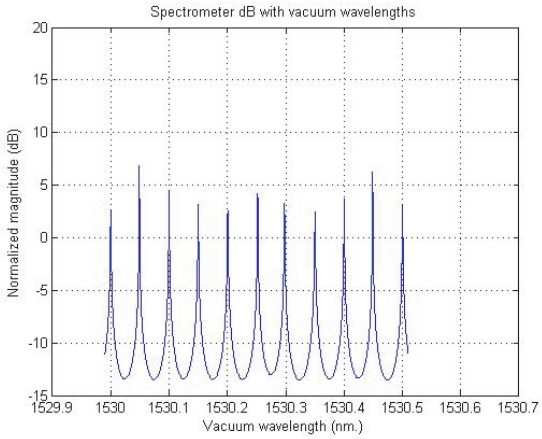

Figure 5. 5:PSD by MUSIC Method for 11 wavelengths

The results with the MUSIC harmonic method are much more satisfying that the results from the AR method. First of all the distance between the peak amplitudes and the valleys is greater than 15 dB, which helps for noise immunity in practice and allow for different levels of peaks to be detected. Also, the peaks are quite narrow, which means that the frequency/wavelength resolution is increased and more peaks could be detected. This suggest that the harmonic model, i.e., complex exponentials + noise is more appropriate than the AR model (white noise exciting an all-pole system) for the specific types of signals that are considered here.

To further investigate the performance of the MUSIC method, 22 wavelength sources were generated instead of 11 sources in the same 1530nm-1530.5nm downsampled range. We can see from figure 5.6 below that the MUSIC method is able to distinguish those 22 peaks.

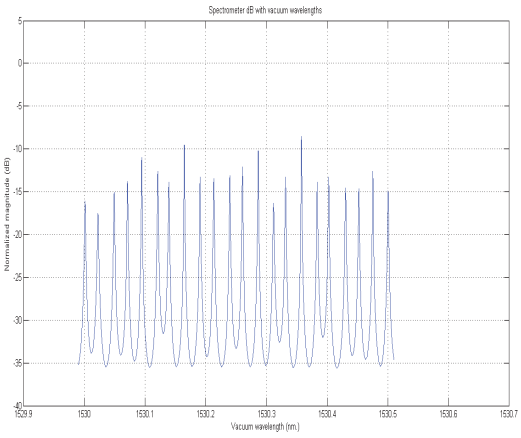

Figure 5. 6:PSD by MUSIC method with 22 wavelengths for same downsampled range 1530nm-1530.5nm

We also found that if we further increase the number of wavelengths in the 1530nm-1530.5nm range (e.g. > 25) the MUSIC methods stops to perform satisfactorily, probably because of numerical issues.

One disadvantage of the MUSIC method (and parametric methods in general) is that there is more variation and uncertainty over the amplitude values and the center positions of the peaks [PRO'96], [UBE'03], [SUB'06], compared to non-parametric methods. We can clearly distinguish the peaks, but their absolute value may easily vary by at least a few dBs.

As mentioned earlier, parametric methods work better when the appropriate model order is selected. In this case, it means the number of peaks that we are supposed to detect in the signal. In practice it is not always possible to know this information a priori.

Phenomena such as line splitting or spurious peaks may happen when there is a mismatch between the model order and the characteristics found in the actual data. Figure 5.7 illustrates the line splitting effect. In this setup a model order 22 was used for a signal that has 11 peaks (laser wavelength) over the considered bandwidth.

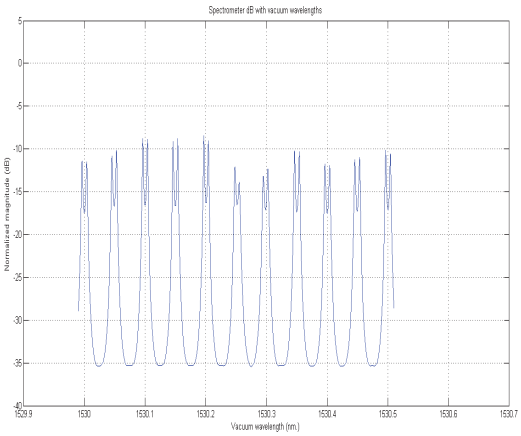

Figure 5. 7:Line splitting effect for MUSIC method

In above figure, we see clearly that the 11 wavelengths are "line splitted" into 2 wavelengths each. Some smoothing of the above figure could also be done to reduce the impact of the line splitting. But nevertheless, this illustrates that knowledge about the model order, i.e., the number of lines or peaks to be detected, is quite important.

5.2 Comparison of results of parametric and non-parametric methods

Consider the case of two laser sources at 1530 nm and 1530.010 nm, i.e., spacing between the two laser sources is 10 pm. For the MUSIC method and the AR Yule-Walker method, the model order was selected as 2 with a rectangular window and the signal was downsampled to the range 1529.98 nm to 1530.03nm. For the MUSIC method we get the following PSD estimate as in figure 5.8.

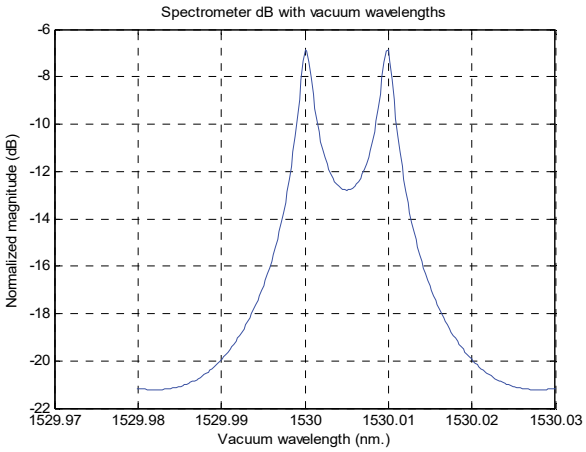

Figure 5.8:MUSIC method for 2 peaks

For the AR Yule-Walker method we get the following PSD estimate as in figure 5.9.

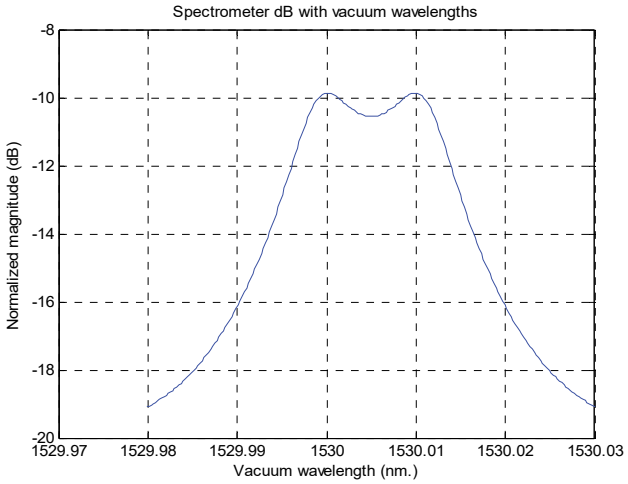

Figure 5.9:Yule-Walker method for 2 peaks at 1530 nm and 1530.010 with order 2

It can be seen that the peaks in the Yule Walker AR method are not as narrow or sharp as in the MUSIC method.

For the same signal, the result of Welch non-parametric PSD estimation using a rectangular window is shown below, with a zoom FFT computation downsampled to 1270nm to 1680nm and zoomed around 1530 nm.

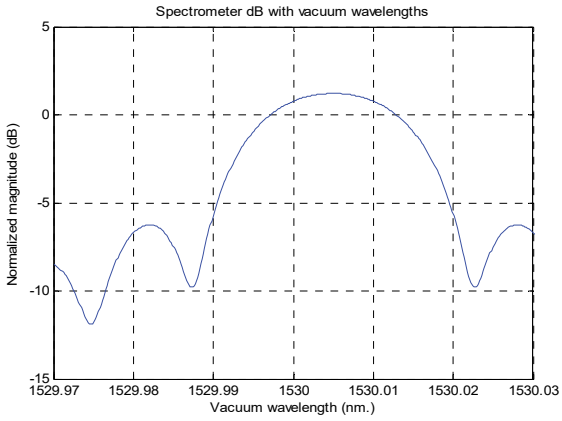

Figure 5.10:FFT method with rectangular window with 2 peaks at downsampled range 1270 nm-1680nm

Similarly, for the same signal the result of Welch non-parametric PSD estimation using a Hamming window is shown below.

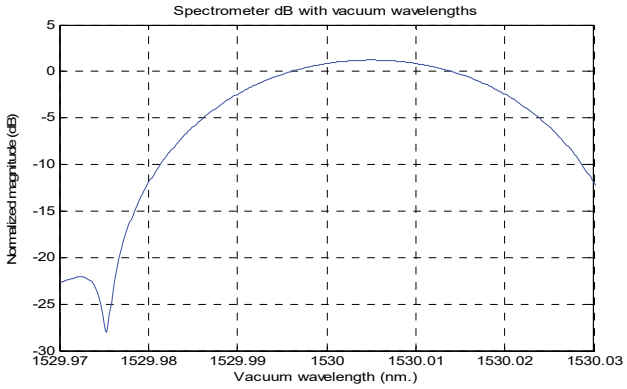

Figure 5.11:FFT method with Hamming window with 2 peaks at downsampled range 1270 nm-1680nm

From the above figures, in this case the MUSIC and AR Yule-Walker parametric PSD estimation method allows to see the two sources, while the FFT method (Welch non-parametric PSD estimation method) using either the rectangular window or the Hamming window (i.e., windows with the best resolution, especially the rectangular window which has the best resolution) cannot distinguish the two sources. Thus the MUSIC method and the AR Yule-Walker method can provide an improved resolution under these conditions.

Case of two laser sources which are spaced very closely at 1530nm and 1530.001nm with a spacing of 1pm was considered. For the PSD estimate obtained from the MUSIC method as shown in Fig. 5. and Fig. 5., a model order of 2 and a rectangular window were used, for a downsampled waveband from 1529.98 nm to 1530.27 nm. For the FFT method, a zoom-FFT with a downsampled wavelength range of 1270 nm to 1680 nm was used, and zoomed around 1530 nm.

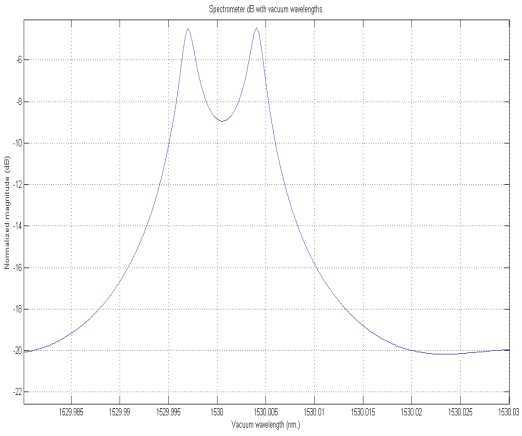

Figure 5.12: MUSIC method for 2 peaks

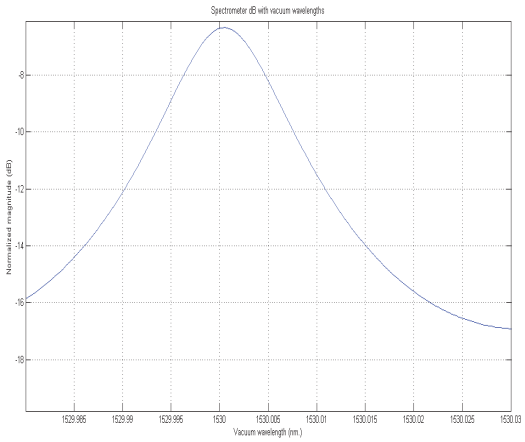

Figure 5.13:Yule-Walker method for 2 peaks at 1530 nm and 1530.001 with order 2

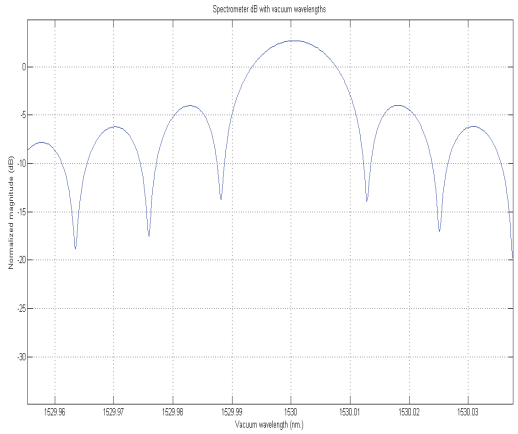

Figure 5.14:FFT method with Rectangular window with 2 peaks at downsampled range 1270 nm-1680nm

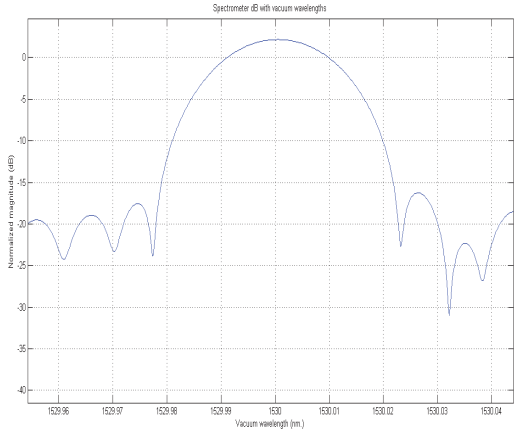

Figure 5.15:FFT method with Hamming window with 2 peaks at downsampled range 1270 nm-1680nm

For the case considered above, it can be seen that for extremely closely spaced wavelengths such as at a distance of 1pm, MUSIC method is able to produce a PSD estimate with 5 dB distance between peak and valley where as Yule-Walker method and FFT method are not able to distinguish the peaks at all. But the only problem associated with MUSIC method is that wavelength position is not accurate as there is a shift in an actual wavelength positions around 1530 nm.

Another case was considered with six laser sources from 1530 nm to 1530.25 nm, with a spacing of 50 pm. In this case the MUSIC method allows to see peaks with about 15 dB between the peak values and the valleys between the peaks (Figure 5.12). The AR Yule-Walker method and the FFT method with rectangular window only provides about 5 dB between the peak values and the valleys (Figure 5.13, Figure 5.14). The FFT method with Hamming window provides about 15 dB between the peak values and the valleys, but the peaks are at the limit of overlapping with each other (Figure 5.15). For the PSD estimate obtained from the MUSIC method as shown in Fig. 5.12 and Fig. 5.13, a model order of 6 and a rectangular window were used, for a downsampled waveband from 1529.98 nm to 1530.27 nm. For the FFT method, a zoom-FFT with a downsampled wavelength range of 1270 nm to 1680 nm was used, and zoomed around 1530 nm.

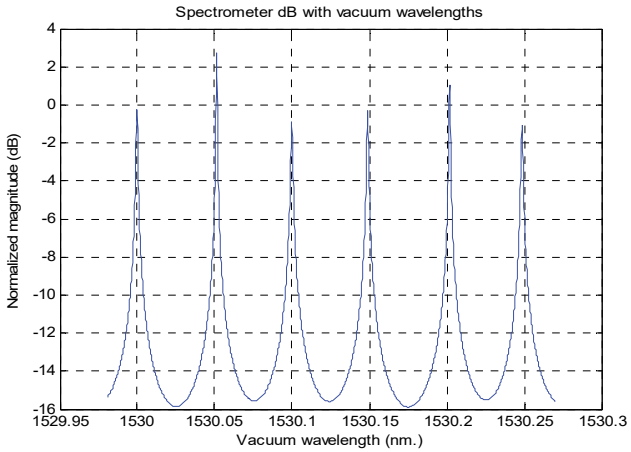

Figure 5.16:MUSIC method for 6 peaks in downsampled range 1529.98nm-1530.27nm

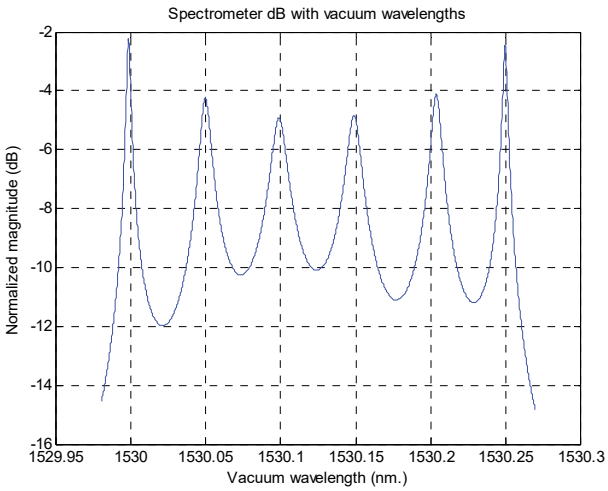

Figure 5.17:Yule Walker AR method for 6 peaks in downsampled range 1529.98nm-1530.27nm.

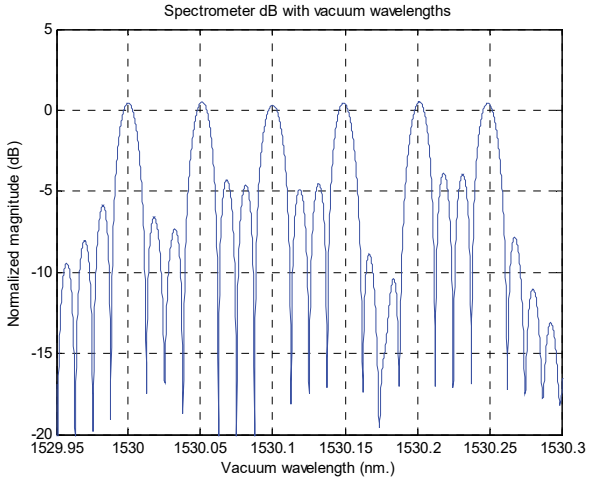

Figure 5.18:Zoom FFT for 6 peaks with rectangular window

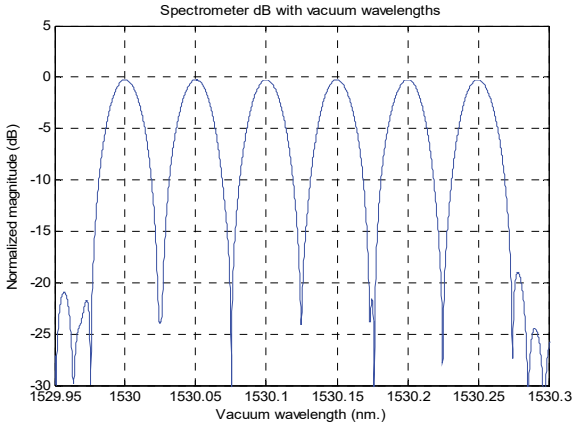

Figure 5.19:Zoom FFT for 6 peaks with Hamming window

For the next case, the number of laser sources was increased from 6 to 15 from 1530 nm to 1530.25 nm with a spacing of 17.9 pm between each laser source. In this case the MUSIC method is able to detect the 15 sources with 5-10 dB between the peak values and the valleys between the peaks (Figure 5.16). The AR Yule-Walker method is not capable to detect the peaks (Figure 5.17). The FFT method with rectangular window can also detect the 15 sources, but the distance between the peak values and the valleys is only about 2-3 dB (Figure 5.18 left). The FFT method with Hamming window cannot detect the 15 sources (Figure 5.18 right). For the MUSIC method and the AR Yule-Walker method, the model order used was 15 with a rectangular window, and the wavelength band selected had a range of 1529.98 nm to 1530.27 nm. For the FFT method, a zoom-FFT with a downsampled wavelength range of 1270 nm to 1680 nm was used, and zoomed around 1530 nm.

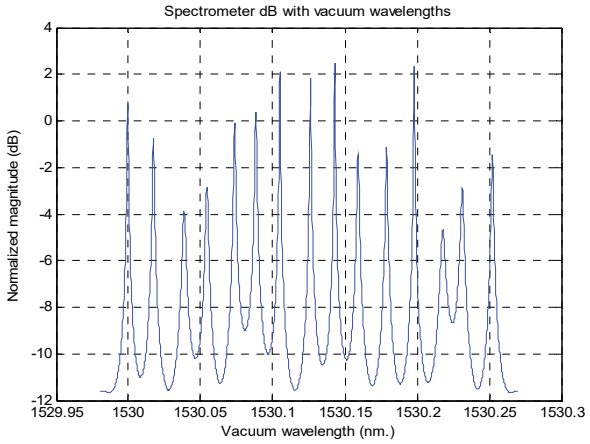

Figure 5.20:MUSIC method with 15 peaks in a range of 1529.98 nm to 1530.27 nm.

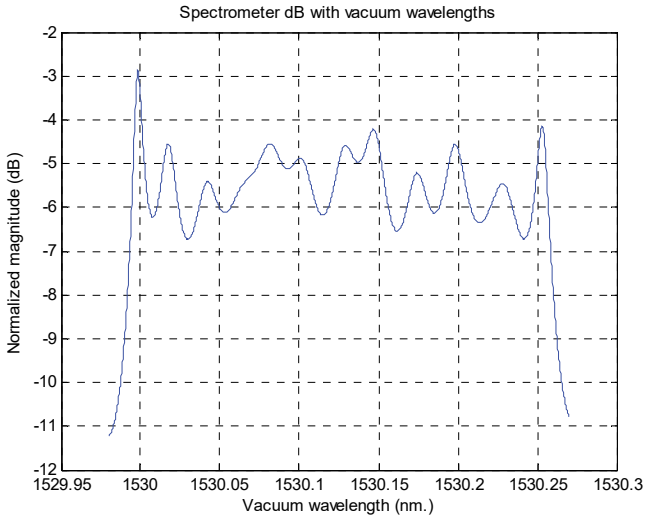

Figure 5.21:Yule Walker AR method with 15 peaks in a range of 1529.98 nm to 1530.27 nm

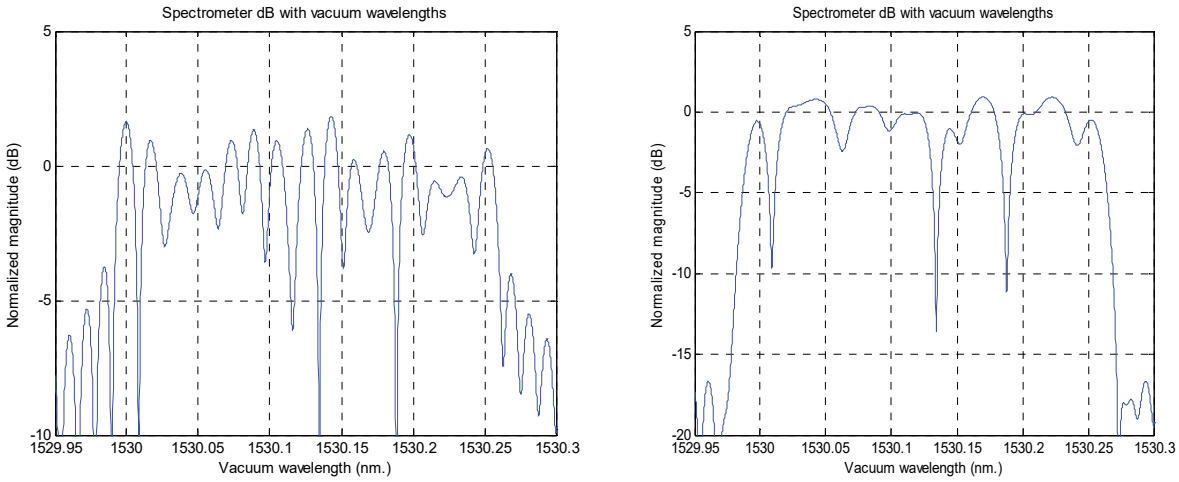

Figure 5.22:FFT with rectangular window and Hamming window respectively for 15 peaks

5.3 Mixing of results from different PSD estimation methods

We consider first the case of three laser sources with two closely located sources at 1531 nm and 1531.015 nm with 15 pm spacing and one weak source which is 60 dB below at a larger distance of 500 pm.

The following figures show the results of FFT-based power spectrum estimation using the rectangular, Hamming, flattop, Blackman, and Kaiser windows, respectively, with decreasing performance in frequency resolution and increasing performance in spectral leakage characteristics. We can see that in the first two figures (especially the first one with the rectangular window), it is possible to distinguish the two closely located strong peaks, but it is absolutely impossible to distinguish the lower peak near -60 dB. The last figure for a Kaiser window with beta parameter 20 is the only one where it is possible to distinguish the weak peak. However, the frequency resolution is poor in that last figure, and it is not possible to clearly distinguish the two strong peaks.

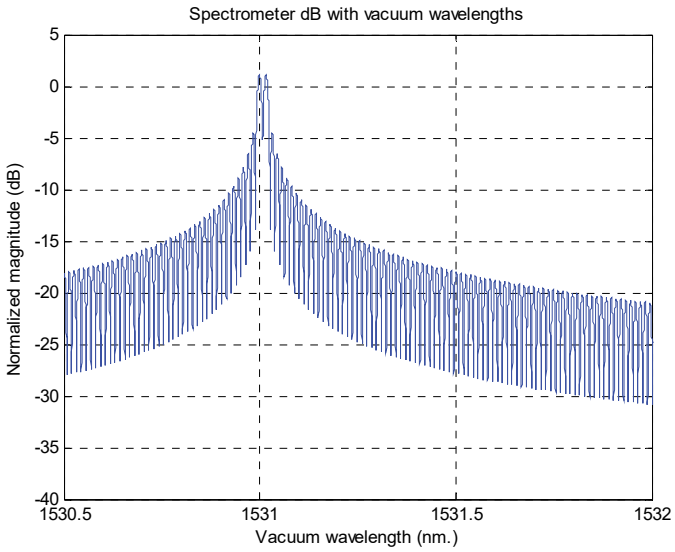

Figure 5.23:FFT method, Rectangular window, downsampled waveband 1530 nm to 1565 nm (zoomed around 1531 nm)

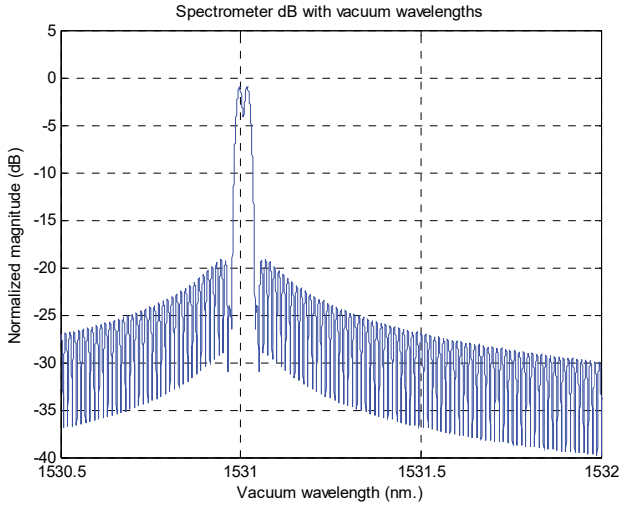

Figure 5.24:FFT method, Hamming window, downsampled waveband 1530 nm to 1565 nm (zoomed around 1531 nm)

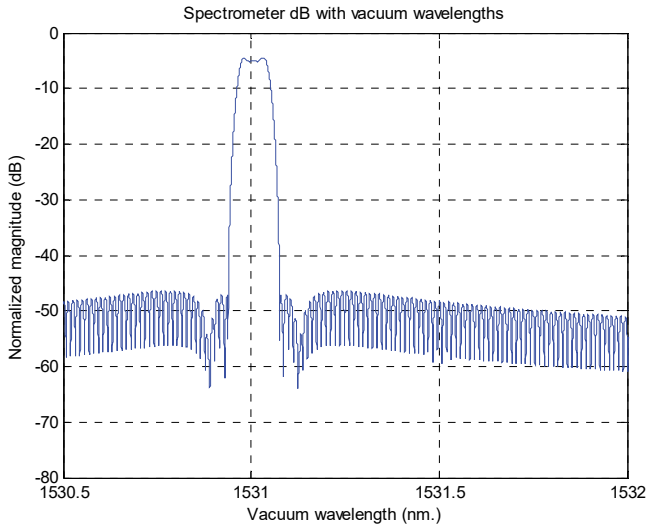

Figure 5.25:FFT method, flattop window, downsampled waveband 1530 nm to 1565 nm (zoomed around 1531 nm)

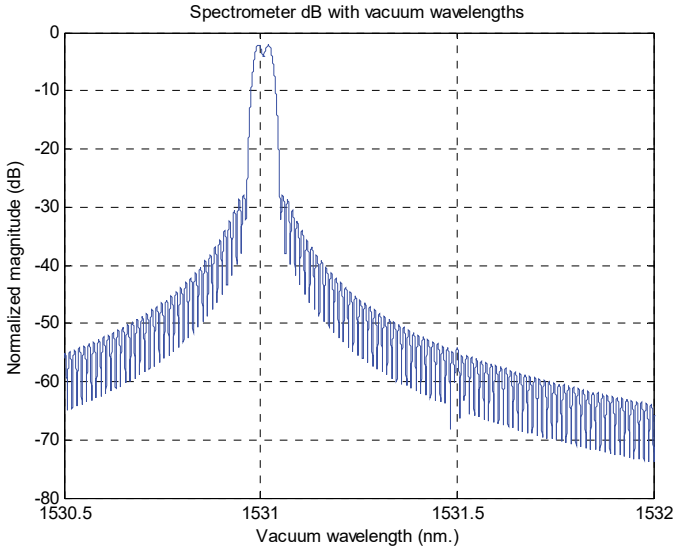

Figure 5.26:FFT method, Blackman window, downsampled waveband 1530 nm to 1565 nm (zoomed around 1531 nm)

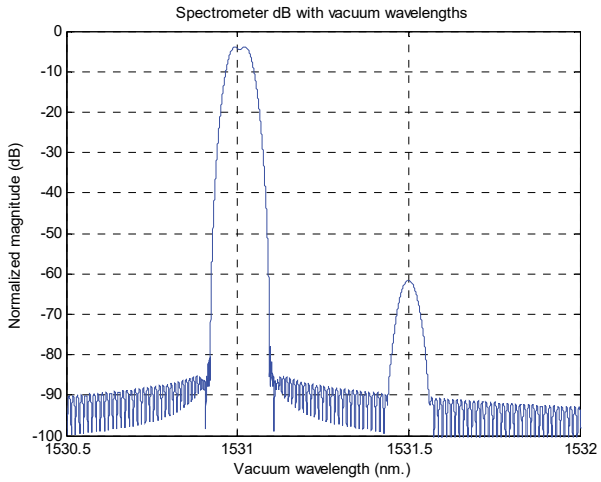

Figure 5.27:FFT method, Kaiser window, downsampled waveband 1530 nm to 1565 nm (zoomed around 1531 nm)

The following figure shows the result of the MIX FFTs method, where the results of the rectangular window giving good frequency resolution and the results of the Kaiser window good spectral leakage characteristics are combined in a single display. It then becomes possible to see in the same figure the two strong peaks and the weaker peak. However, the figure should only be used as an indication for the presence of peak components, not for the measurement of the peak amplitude levels e.g. the level of the weaker peak no longer corresponds to its original level.

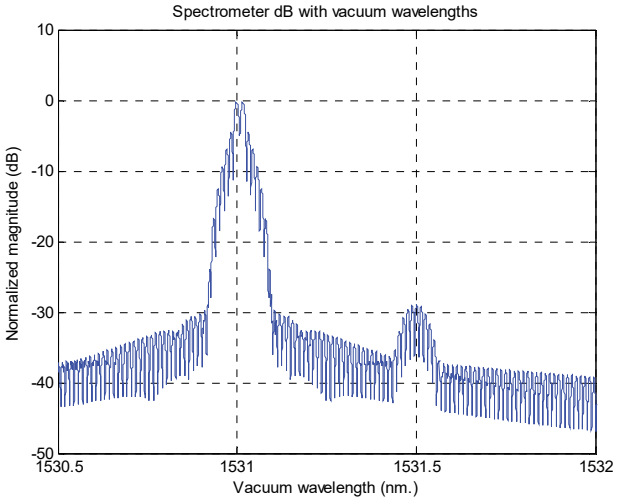

Figure 5.28:MIX FFTs method, mix of results from rectangular window (75%) and Kaiser window (25%), downsampled waveband 1530 nm to 1565 nm (zoomed around 1531 nm)

Next experiments were conducted to investigate the performance of the "MIX FFT and MUSIC" method. For this experiment, six laser sources from 1530 nm to 1530.25 nm with a spacing of 50 pm were used (same as previously used setup). For the MUSIC method, a model order 6 with a downsampled waveband of 1529.98 nm to 1530.27 nm was used with rectangular window and the result is as follows.

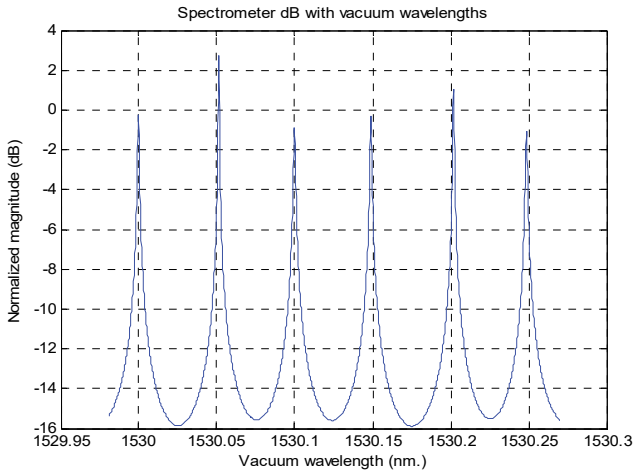

Figure 5.29:MUSIC method for 6 peaks in downsampled range 1529.98 nm to 1530.27 nm with rectangular window.

For the FFT method, a zoom-FFT with a downsampled wavelength range of 1270 nm to 1680 nm was used, and zoomed around 1530 nm. The result for a rectangular window is presented below.

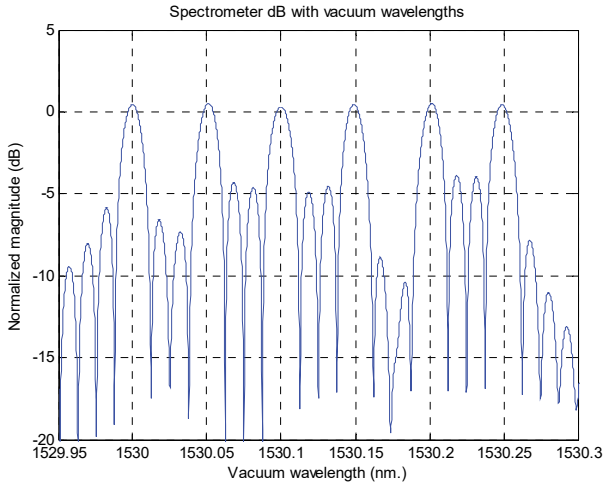

Figure 5.30:FFT method, rectangular window, downsampled waveband 1270 nm to 1680 nm (zoomed around 1530 nm)

Next, the result for the "MIX FFT and MUSIC" method is presented below, combining the results of the two previous figures.

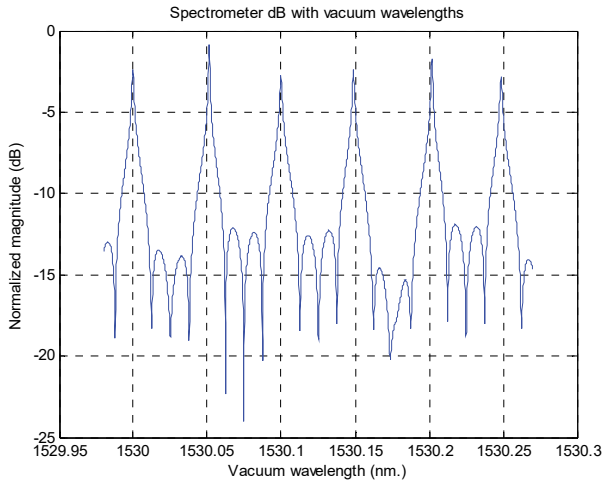

Figure 5.31:MIX FFT and MUSIC (model order = 6), rectangular window, downsampled waveband 1529.98 nm to 1530.27 nm

It can be seen that the result of the above figure is indeed a 50% / 50% mix of the two previous figures. The usefulness of the "MIX FFT and MUSIC" method is to combine the narrow peaks of the MUSIC algorithms with the robustness of a non-parametric Welch estimate.

5.4 Further comparisons for the best working methods

According to discussions and results from the previous sections, it is clear that the parametric methods such as the AR Yule-Walker method and harmonic methods such as the MUSIC method can potentially provide a better frequency resolution to detect the peaks in interferometer signals. The MUSIC method seems to provides better results than AR Yule-Walker method in terms of frequency resolution. But as will be shown in this section, there are some cases where the Yule-Walker method gives better results than the MUSIC method, i.e., more robust results. These cases will be discussed in this section.

Although the previous results were showing advantages of using the MUSIC algorithm for spectral analysis, there are however important limitations to the use of this algorithm. The main problem is that the appropriate model order needs to be known, which normally corresponds to the number of sources (peaks) to be detected in the spectrum. However, if the number of active sources to detect is unknown, it is difficult to use a trial and error method to determine the best model order, because when a model order higher than the number of active sources is used, the method will create artificial peaks which appear as seemingly valid detected peaks. This is the phenomena of "spurious peaks" previously introduced in the thesis, which

are peaks that are artificially created by the method; another related phenomenon is the "line splitting" effect, where valid peaks are split into two closely located peaks.

To illustrate the problem of spurious peaks / line splitting, the case of 2 laser sources at 1530 nm and 1530.010 nm (spacing of 10pm) is considered again, where the MUSIC method produces the following result.

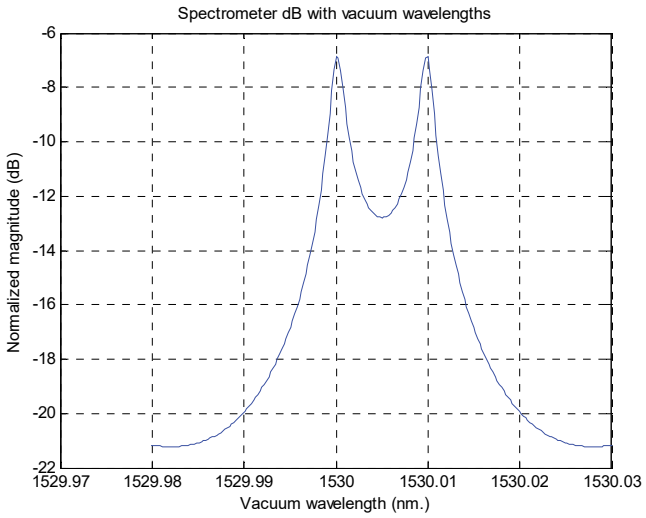

Figure 5.32:MUSIC method, model order = 2, rectangular window, downsampled waveband 1529.98 nm to 1530.03 nm, laser sources at 1530 nm and 1530.010 nm.

Now if the source at 1530.010 nm is turned off and only one source remains at 1530 nm, if the analysis is performed with the same setup (especially with model order set to 2), the following result is obtained.

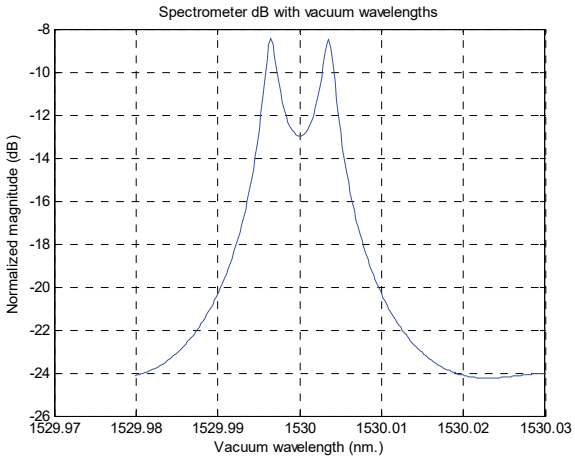

Figure 5.33:MUSIC method, model order = 2, rectangular window, downsampled waveband 1529.98 nm to 1530.03 nm, laser source at 1530 nm.

Although there has been a shift in the frequencies detected (now centered around 1530 nm), this result would typically not be acceptable, as it clearly shows 2 peaks although there is only one source active at 1530 nm. This is because of line splitting.

The Yule-Walker AR method behaves better for this scenario, as shown in Figures 5.28 and 5.29 (with the same settings used as for the MUSIC algorithm).

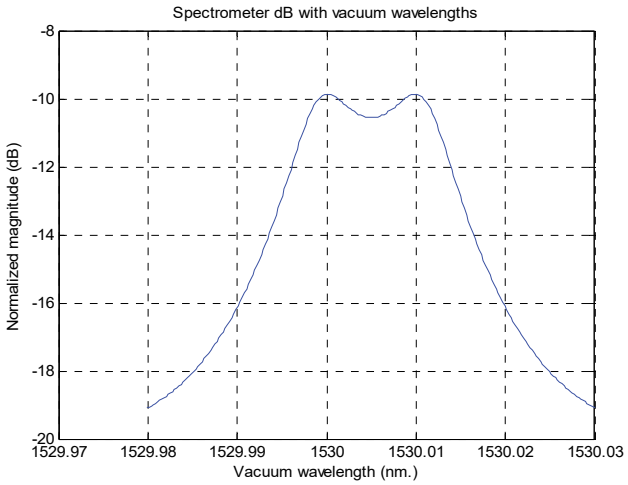

Figure 5.34:Yule-Walker method, model order = 2, rectangular window, downsampled waveband 1529.98 nm to 1530.03 nm, laser sources at 1530 nm and 1530.010 nm.

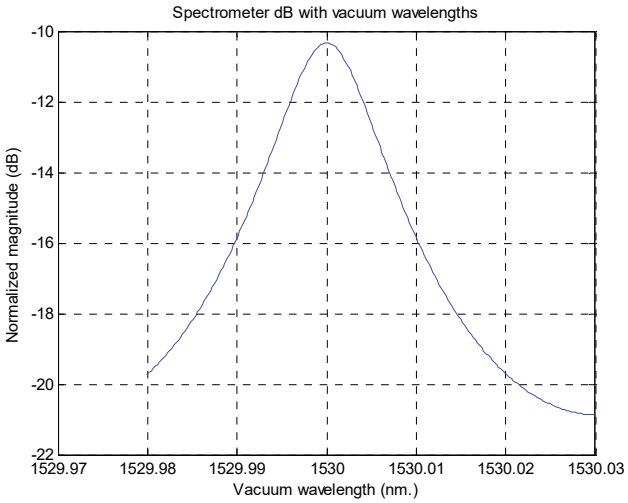

Figure 5.35:Yule-Walker method, model order = 2, rectangular window, downsampled waveband 1529.98 nm to 1530.03 nm, laser source at 1530 nm.

Unlike the MUSIC method, the Yule-Walker method with order 2 displays the right number of peaks, i.e., if only one source is active then it only displays one peak, thus it can be used to improve the frequency resolution for the case of two closely located peaks, compared to the FFT-based method (Figures 5.10 and 5.11).

Even when the correct model order is used, another disadvantage of the results provided by the MUSIC method is that the center frequencies of the detected peaks are not as accurate as in the case of the FFT methods. This also applies for the amplitude of the peaks, which are not very reliable.

Chapter 6 Discussion

As discussed in Chapter 1, this thesis is about evaluating PSD estimation methods to distinguish and detect the active laser sources at any given time from the signal provided by a Michelson interferometer. The most important factor to display the peaks in the spectrum is the frequency resolution. For this purpose, different methods were evaluated after doing some literature survey on non-parametric and parametric PSD estimation methods. The criteria set for evaluating performance of these methods was the ability of these PSD methods to produce a display which will allow us to observe visually the presence of a peak in the estimated spectrum. After doing some experiments in Chapter 5, it was found that parametric methods (especially the MUSIC method) can provide a better frequency resolution than non-parametric methods. However there are some factors which have to be considered before applying parametric methods:

1. The number of peaks (i.e., model order) to be detected should not be too large, otherwise numerical issues prevent the method to perform properly. For the MUSIC method or the Yule Walker AR method, model orders above 20 were seldom found to lead to appropriate results, and it is better to use smaller model orders.
2. With parametric methods, only a small part of the waveband can be analyzed at a given time. For interferometer signals with several peaks (e.g. over 20), downsampling to several waveband areas containing 20 peaks or less would need to be performed.
3. The MUSIC/harmonic method or the Yule Walker/AR method perform much better when the signal to be analyzed contains only the waveband of interest, i.e., downsampled to the relevant waveband area, even if the original interferometer signal contains just a few peaks to be analyzed.
4. In some cases this can lead to extreme downsampling, which needs anti-aliasing lowpass filters with very small passbands, with long filters having a lot of coefficients. This in turn leads to a filter length of the same order than the signal to be filtered for the case considered in this thesis (the interferometer signal with 300,000 samples). This is not an ideal situation, as the resulting filtered signal includes significant transient effects from the filter. Transients are produced in the output signal due to the edge effects from the transitory response of the impulse response of the anti-aliasing lowpass filter. In order to maximize the use of the available information, the experiments were performed on the whole filtered signal, including the transient effects at the beginning and the end of the filtered signal.
5. Wavebands greater than 50 pm were used for the analysis, to limit the size of the downsampling and the effect of the transients in the filtered signal.

6. For cases with significant downsampling, the transient effects at the beginning and at the end of the filtered signal lead to a resulting signal with attenuated values at those edges. Due to this, the impact of further applying a non-rectangular window on the resulting filtered signal became non-significant. So for cases where small wavebands are selected i.e. high downsampling, applying a rectangular window or a non-rectangular window such as Hamming on the downsampled signal will not make much difference for the MUSIC/harmonic method or the Yule Walker/AR method.

Along with these classic methods, two new mixing methods were proposed in this thesis: the MIX FFTs and MIX FFT and MUSIC methods. It is clear that the MIX FFTs method can be used to have both the best frequency resolution available from an FFT method and at the same time good spectral leakage characteristics, by combining the spectra obtained from two or multiple windows. But these benefits come at the expense of accuracy in the levels of the components.

The MIX FFT and MUSIC method may be used for some cases where the peaks to be displayed should have both a narrow frequency resolution and a better robustness than typical parametric PSD estimation methods. The non-parametric FFT method provide the reliable and robust PSD estimation whereas the MUSIC method provides sharp and narrow peaks. These can then be amalgamated to provide robust/reliable results with sharp peaks, by applying equal weights to each method.

Chapter 7 Summary and Conclusion

7.1 Summary of work

The main objective of this thesis was to test in chapter 5 existing PSD estimation techniques along with some new techniques introduced in the thesis to detect peaks in optical signals received through a Michelson interferometer. Although our experiments were performed on synthetic signals, these were generated using realistic scenarios provided by our sponsor company Simbol Test Systems Inc., and the resulting code was delivered to Simbol for integration into their wavemeter product.

Understanding the working of an interferometer, its physics and the mathematics related to it was done through a literature survey. We were able to understand and explain many concepts such as the space sampling, the interference of optical light waves etc. In chapter 2, it was explained that the sampling in the interferometer was done through the mirror movement.

Basics of the periodogram and non-parametric methods were studied in chapter 3. In general, non-parametric methods are used when no or little information is available about the signal. Long data records are often needed in non-parametric methods to obtain the adequate frequency resolution. Non-parametric methods suffer from spectral leakage, although they try to reduce this by using windowing. These methods assume that the autocorrelation of the signal outside the finite data record is zero, which affects the frequency resolution [PER'93], [ZAK'05].

The concepts of parametric PSD estimation methods were presented in chapter 4. With parametric spectrum estimation, it is possible to incorporate a model for the signal generating process in the spectrum estimation algorithm, which can potentially give higher frequency resolution and a more accurate spectrum estimation [ZAK'05], [OPP'09].

To compare non-parametric and parametric PSD estimation methods, experiments with different types of challenging signals were performed in Chapter 5. Results have shown that parametric methods (especially the MUSIC harmonic method) were able to distinguish peaks with a better frequency resolution or with a greater peak and valley distance in dB, compared to FFT-based non-parametric methods. But parametric methods have their own limitations. When the order of the model is increased beyond a certain value, the performance of these methods becomes poorer. They can also suffer from spurious peaks, line splitting, and they show a significant variance in the estimation of the detected frequencies and the levels of these frequencies.

The use of parametric methods can be summarized in following steps:

1) Selecting the appropriate model and model order based on the a priori knowledge of the generation of the measured data;

2) From the measured data estimate the model parameters;

3) From the model estimate, compute the power spectrum estimate.

Though the MUSIC method was found to often lead to better frequency resolution than the AR Yule-Walker method for the types of signals considered in this thesis, it suffers from the problem of line splitting if an appropriate model order is not selected. This may result in not correctly detecting to right number of closely located peaks unless the correct model order is used, and it limits the applicability of the method for such cases.

Parametric methods will likely never produce results which are as predictable or robust as traditional non-parametric methods. In the literature, the term "pseudo-PSD" has been used to describe the fact that the PSD estimates returned by parametric methods differ from the traditional and predictable PSD estimates provided by non-parametric methods. But from the results of this thesis, we can say that they can be a useful complement to traditional methods for the types of signals considered in this thesis, and they can provide better frequency resolutions under some conditions.

The newly contributed methods in this thesis are the MIX FFTs and the MIX FFT and MUSIC methods. The MIX FFTs is useful in detecting simultaneously close peaks and distant weak peaks in a spectrum, which requires both a good frequency resolution and good spectral leakage properties. This is achieved by averaging two FFTs spectra estimated using windows with different spectral leakage characteristics. Though this method can successfully detect and display weak peaks, it lacks the ability to show their true level values. For the MIX FFT and MUSIC method, the resulting spectrum displayed will be more dependable and robust compared to purely parametric spectra, while at the same time showing sharp peaks and good frequency resolution.

7.2 Future Work

In parametric methods and harmonic methods some limitations may arise due to the limitation on selecting the right model order. Model order estimation has been a widely studied area of research and some modern techniques could be combined with the parametric PSD estimation techniques of this work, leading to potentially more robust performance. In addition, there are a few classes of PSD estimation methods which

have not been tested in this work. For example, further investigations could be done with the use of other AR models such as the Capon method and line spectra methods.

References

[AYE'03] Bulent Ayhan, Mo-Yuen Chow, H. Joel Trussell, Myung-Hyun Song, "A Case Study on the Comparison of Non-parametric Spectrum Methods for Broken Rotor bar Fault Detection", Proc. IEEE IECON, pp. 2835-2840, 2003

[BAB'14] Behtash Babadi and Emery N. Brown, "A Review of Multitaper Spectral Analysis", IEEE Transactions on Biomedical Engineering, Vol.61, No.5, May 2014

[BEL'01] Maurice Bellanger, "Adaptive Digital Filters (Signal Processing and Communications)", Marcel Dekker, pp.357-378, 2001

[BRO'06] Piet M.T. Broersen, "Automatic Autocorrelation and Spectral Analysis", Springer, pp.29-221, 2006

[CAR'82] James A. Cardow, "Spectral Estimation: An Overdetermined Rational Model Equation Approach", Arizona State Univesity, Sept. 1982

[CAS'11] Francis Castanie, "Digital Spectral Analysis: parametric, non-parametric and advanced methods", Wiley, pp.145-166, 2011

[CHA'90] B. Fong Chao, "On the use of Maxmum Entropy/Autoregressive Spectrum in Harmonic Analysis of Time Series", Pageoph, Vol.134, No.2, 1990

[CHO] T.Chonavel, "Statistical Signal Processing Modelling and Estimation", Springer-Verlag, pp.139-184

[COL] A.R. Collins, Miscellaneous Technical Articles, Available: http://www.arc.id.au/ZoomFFT.html

[GOL] Nina Golyandina, Anatoly Zhigljavsky, "Singular Spectrum Analysis for Time Series", Springer, pp. 104-108

[HAY'97] Monson H. Hayes, "Statistical Digital Signal Processing and Modeling", John Wiley & Sons, pp.391-465, 1997

[HUA'14] Junyou Huang, "Study of Autoregressive (AR) Spectrum Estimation Algorithm for Vibration Signals of Industrial steam turbines", International Journal of Control and Automation, Vol.7, No.8, pp.349-362, 2014

[KAU'01] J.Kauppinen, J.Partanen, "Fourier Transforms In Spectroscopy", Wiley, pp.77-99, 2001

[MAN'05] Dimitris G. Manolakis, Vinay K. Ingle, Stephen M. Kogon, "Statistical and adaptive signal processing: Spectral Estimation, Signal Modeling, Adaptive Filtering and Array Processing", Artech House, pp.195-254, 445-493, 2005

[MAR'01] Rainer Martin, "Noise Power Spectral Density Estimation Based on Optical Smoothing and Minimum Statistics", IEEE transactions on speech and audio processing, Vol.9, No.5, July 2001

[MIC] The Michelson Interferometer, Available: http://www.physics.umd.edu/courses/Phys375/AnlageFall06/Lab4Michelson.pdf

[MUL] Multiline Optical Channel Analyzer, Available: http://www.exfo.com/Documents/TechDocuments/Specification_Sheets/EXFO_spec-sheet_WA-7600-7100_en.pdf

[OPP'09] Alan V. Oppenheim, Ronald W. Schafer, "Discrete Time Signal Processing", Pearson, pp.890-926, 2009

[ORF] Sophocles J. Orfanidis, "Introduction to Signal Processing", Available: www.ece.rutgers.edu/~orfanidi/i2sp

[PER'93] Donald B. Percival, Andrew T. Walden,"Spectral Analysis For Physical Applications:Multitaper and Conventional Univariate Techniques", Cambridge University Press,pp.391-451, 1993

[PER'06] Luis A.Pereira, Denis Fernandes, Daniel S. Gazzana, Fausto B. Libano and Sergio Haffner, "Performance Evaluation of Nonparametric, Parameric, and the MUSIC Methods to Detection of Rotor Cage Faults of Induction Motors", Proc. 32nd Annu. Conf IEEE Ind. Electron, pp. 5005-5010, 2006

[PRA'85] A. V. Prabhu, V. K. Aatre, T.Soumini and S. A. Karipel, "Frequency Zooming Techniques for High Resolution Spectrum Analysis", Def Sci J, Vol.35, pp.281-285, July 1985

[PRO'96] John .G. Proakis, Dimitris .G. Manolakis, "Digital Signal Processing- Principles,Algorithms and Applications", Prentice-Hall, pp.896-959, 1996

[STO'05] Peter Stoica, Randolph L. Moses, "Spectral Analysis of Signals", Prentice Hall, pp.23-131, 2005

[SUB'06] Abdulhamit Subasi, Ergun Ercelebi, Ahmet Alkan, Etem Koklukaya, "Comparison of subspace-based methods with AR parametric methods in epileptic seizure detection", Computers in Biology and Medicine, Vol.36, pp.195-208, 2006

[SUB'07] Abdulhamit Subasi, "Selection of optimal AR spectral estimation method for EEG signals using Cramer-Rao bound", Computers in Biology and Medicine, Vol.37, pp.183-194, 2007

[TCH'08] Dr. Gleb.V. Tcheslavski, "Lecture 08:Spectrum estimation-nonparametric methods", 2008, Available: http://www.ee.lamar.edu/gleb/adsp/Lecture%2008%20-%20Nonparametric%20SE.pdf

[TCH'09] Dr. Gleb.V. Tcheslavski, "Lecture 09:Spectrum estimation-parametric methods", 2009, Available: http://www.ee.lamar.edu/gleb/adsp/Lecture%2009%20-%20Parametric%20SE.pdf

[TEC'80] Technical Review: To Advance Techniques in Acoustical, Electrical and Mechanical Measurement, Bruel & Kiaer, No.2, 1980

[THO'82] D. J. Thomson, "Spectrum estimation and harmonic analysis", Proc.IEEE, vol.70, No.9, pp.1055-1096, Sep.1982

[UBE'03] Elif Derya Ubeyli, Inan Guler, "Comparison of eigenvector methods with classical and model-based methods in analysis of internal carotid arterial Doppler signals", Computers in Biology and Medicine, Vol.33, pp.473-493, 2003

[UBE'04] Elif Derya Ubeeyli, Inan Guler, "Selection of optimal spectral estimation method for internal carotid arterial Doppler signals using Cramer-Rao bound", Elsevier, Computers and Electrical Engineering, Vol.30, pp. 491-508, 2004

[UCD] UCDAVIS, "How an FTIR spectrometer operates", Available: http://chem.libretexts.org/Core/Physical_and_Theoretical_Chemistry/Spectroscopy/Vibrational_Spectroscopy/Infrared_Spectroscopy/How_an_FTIR_Spectrometer_Operates

[WEL'67] Peter D. Welch, "The Use of Fast Fourier Transform for the Estimation of Power Spectra: A Method Based on Time Averaging Over Short, Modified Periodograms", IEEE Trans. Audio and Electroacoust., Vol.AU-15, pp.70-73, June 1967

[YUE'07] Peng Yuexiang, Wang Liqiang and Linli, "Study of Fourier Transform Spectrometer based on Michelson Interferometer Wave-meter", Proc.of SPIE, Vol.6837, 68370T-2, 2007

[ZAK'05] A.Zaknich, "Principles of Adaptive Filters and Self-learning Systems", Springer, pp.197-223, 2005